Sources and formation of carbonaceous aerosols in Xi'an, China: primary emissions and secondary formation constrained by radiocarbon

Haiyan Ni[1,2,3], Ru-Jin Huang[1*], Junji Cao[1], Jie Guo[1], Haoyue Deng[2], Ulrike Dusek[2]

[1]State Key Laboratory of Loess and Quaternary Geology, Key Laboratory of Aerosol Chemistry and Physics, Center for Excellence in Quaternary Science and Global Change, Institute of Earth Environment, Chinese Academy of Sciences, Xi'an, 710061, China

[2]Centre for Isotope Research (CIO), Energy and Sustainability Research Institute Groningen (ESRIG), University of Groningen, Groningen, 9747 AG, the Netherlands

[3]University of Chinese Academy of Sciences, Beijing, 100049, China

Correspondence to: rujin.huang@ieecas.cn

Abstract. To investigate the sources and formation mechanisms of carbonaceous aerosols, a major contributor to severe particulate air pollution, radiocarbon (^{14}C) measurements were conducted on aerosols sampled from November 2015 to November 2016 in Xi'an, China. Based on the ^{14}C content in elemental carbon (EC), organic carbon (OC) and water-insoluble OC (WIOC), contributions of major sources to carbonaceous aerosols are estimated over a whole seasonal cycle: primary and secondary fossil sources, primary biomass burning, and other non-fossil carbon formed mainly from secondary processes. Primary fossil sources of EC were further sub-divided into coal and liquid fossil fuel combustion by complementing ^{14}C data with stable carbon isotopic signatures.

The dominant EC source was liquid fossil fuel combustion (i.e., vehicle emissions), accounting for 64% (median; 45–74%, interquartile range) of EC in autumn, 60% (41–72%) in summer, 53% (33–69%) in spring and 46% (29–59%) in winter, respectively. An increased contribution from biomass burning to EC was observed in winter (~28%) compared to other seasons (warm period; ~15%). In winter, coal combustion (~25%) and biomass burning equally contributed to EC, whereas in the warm period, coal combustion accounted for a larger fraction of EC than biomass burning. The relative contribution of fossil sources to OC was consistently lower than that to EC, with an annual average of $47 \pm 4\%$. Non-fossil OC of secondary origin was an important contributor to total OC ($35 \pm 4\%$) and accounted for more than half of non-fossil OC ($67 \pm 6\%$) throughout the year. Secondary fossil OC (SOC$_{fossil}$) concentrations were higher than primary fossil OC (POC$_{fossil}$) concentrations in winter, but lower than POC$_{fossil}$ in the warm period.

Fossil WIOC and water-souble OC (WSOC) have been widely used as proxies for POC$_{fossil}$ and SOC$_{fossil}$, respectively. This assumption was evaluated by (1) comparing their mass concentrations with POC$_{fossil}$ and SOC$_{fossil}$, and (2) comparing ratios of fossil WIOC to fossil EC to typical primary OC to EC ratios from fossil sources including both coal combustion and vehicle emissions. The results suggest that fossil WIOC and fossil WSOC are probably a better approximation for primary and secondary fossil OC, respectively, than POC$_{fossil}$ and SOC$_{fossil}$ estimated using the EC tracer method.

1. Introduction

Carbonaceous aerosols are an important component of $PM_{2.5}$ (particles with aerodynamic diameter <2.5 μm), constituting typically 20–50% of $PM_{2.5}$ mass in many urban areas in China (Cao et al., 2012; R. J. Huang et al., 2014; Tao et al., 2017). The total carbon content of carbonaceous aerosols (TC) is operationally classified into elemental carbon (EC) and organic carbon (OC) (Pöschl, 2005). EC is emitted as primary aerosols from incomplete combustion of biomass (e.g., wood, crop residues, and grass) and fossil fuels (e.g., coal, gasoline and diesel). In addition to these combustion sources, OC has other non-combustion sources, for example, biogenic emissions, cooking, etc. Unlike EC that is exclusively emitted as primary aerosols, OC includes both primary and secondary OC (POC and SOC, respectively), where SOC is formed in the atmosphere by chemical reaction and gas-to-particle conversion of volatile organic compounds (VOCs) from non-fossil (e.g., biomass burning, biogenic emissions, and cooking) and fossil sources (Jacobson et al., 2000; Kanakidou et al., 2005; Hallquist et al., 2009). Moreover, OC can be separated into water-soluble OC (WSOC) and water-insoluble OC (WIOC), aaccording to water solubility of OC.

High concentrations of carbonaceous aerosols have been observed during severe air pollution events in China (R. J. Huang et al., 2014; Elser et al., 2016; Liu et al., 2016a, 2016b). Knowledge and understanding of the sources and formation processes of carbonaceous aerosols, which remain unclear due to the complicated chemical composition, are highly needed to improve air quality. Clear-cut separation between fossil and non-fossil sources of carbonaceous aerosols can be successfully achieved by radiocarbon measurement (Gustafsson et al., 2009; Szidat et al., 2009; Dusek et al., 2013). Radiocarbon (^{14}C) source apportionment exploits the fact that carbonaceous aerosol emitted from fossil sources (e.g., coal combustion, vehicle emissions) does not contain ^{14}C, whereas carbonaceous aerosol released from non-fossil (or "contemporary") sources has a typical contemporary ^{14}C signature. Radiocarbon studies show that a sizeable fraction of carbonaceous aerosols is from non-fossil origins, even for aerosols collected in urban areas (Heal, 2014; Cao et al., 2017). For example, Zhang et al. (2015b) found that 48 ± 9% total carbonaceous aerosols were contributed by non-fossil sources in urban areas of 4 large Chinese cities in winter of 2013. [14]C measurements conducted in early winter in 10 Chinese cities show that on average 65 ± 7% total carbonaceous aerosols were derived from non-fossil sources (Liu et al., 2017). When ^{14}C analysis is conducted for OC and EC separately, contributions from biomass burning and other non-fossil sources to carbonaceous aerosols can be separated for a more comprehensive source apportionment.

[14]C measurements on either WIOC or WSOC can help to separate primary from secondary OC from fossil sources. Fossil sources tend to mainly produce WIOC in primary emissions (Weber et al., 2007; Dai et al., 2015; Yan et al., 2017). Therefore, fossil WIOC ($WIOC_{fossil}$) can be used as a proxy of fossil POC (POC_{fossil}). WSOC can be directly emitted as primary aerosols mainly from biomass burning or produced as SOC. There is evidence that SOC produced through the oxidation of VOCs followed by gas-to-particle conversion contains more polar compounds and thus may be an important source of WSOC (Miyazaki et al., 2006; Sannigrahi et al., 2006; Kondo et al., 2007; Weber et al., 2007). Fossil WSOC

(WSOC$_{fossil}$) therefore is thought to be a good proxy of fossil SOC (SOC$_{fossil}$). ^{14}C analysis of WIOC and WSOC can therefore provide new insights into sources and formation processes of primary and secondary OC, respectively, and has been applied in several source apportionment studies (e.g., Liu et al., 2016a, 2016b; Dusek et al., 2017; Liu et al., 2017). For example, using this approach, Y. L. Zhang et al. (2014) found that secondary fossil OC dominates total fossil OC in a background site in southern China. Measurements in 4 Chinese megacities highlight the importance of secondary formation to both fossil and non-fossil WSOC in severe winter haze episodes, by combining ^{14}C measurements of WSOC with positive matrix factorization of aerosol mass spectrometer data (Zhang et al., 2018).

^{14}C measurements on EC allow direct separation of fossil and biomass burning source contributions. In addition, analysis of the stable carbon isotopic composition (namely the ^{13}C/^{12}C ratio, expressed as δ^{13}C in Eq. 1) of EC can be used to separate fossil sources into coal and liquid fossil fuel combustion (i.e., vehicle emissions), because EC from coal combustion is on average more enriched in the stable carbon isotope ^{13}C compared to liquid fossil fuel combustion (Andersson et al., 2015; Winiger et al., 2015, 2016; Fang et al., 2018). The interpretation of the stable carbon isotope signature for OC source apportionment is more difficult, because OC is chemically reactive and δ^{13}C signatures of OC are not only determined by the source signatures but also influenced by chemical reactions of the organic compounds in the atmosphere (Irei et al., 2011; Pavuluri and Kawamura, 2016).

In this study, one-year PM$_{2.5}$ samples collected from Xi'an, China are investigated. Xi'an is the largest city in northwest China and is also one of the most polluted cities in the world. We present, to our best knowledge, the first ^{14}C measurements covering all four seasons that distinguish fossil and non-fossil contributions to various carbon fractions, including EC, OC, WIOC and WSOC in Xi'an. Fossil sources of EC are further divided into coal and liquid fossil fuel combustion by complementing radiocarbon with the stable carbon isotopic signature. Concentrations of POC$_{fossil}$ and SOC$_{fossil}$ are modeled based on the ^{14}C-apportioned OC and EC and compared with their widely used proxies, i.e., ^{14}C-apportioned WIOC$_{fossil}$ and WSOC$_{fossil}$, respectively.

2. Methods

2.1 Sampling

Sampling was conducted in Xi'an, China from 30 November 2015 to 17 November 2016. PM$_{2.5}$ samples were collected on the rooftop (~10 m) of a two-floor building located at the Institute of Earth Environment, Chinese Academy of Sciences (34.2° N, 108.9° E). This site is a typical urban background site surrounded by residential and education areas. The 24 h integrated PM$_{2.5}$ samples were collected from 10:00 to 10:00 the next day (local standard time, LST). PM$_{2.5}$ samples were collected on pre-baked (780 °C for 3 h) quartz fiber filter (QM/A, Whatman Inc., Clifton, NJ, USA, 20.3 cm × 25.4 cm) using a high-volume sampler (TE-6070 MFC, Tisch Inc., Cleveland, OH, USA) at a flow rate of 1.0 m^3 min^{-1}. Field blank

filters were treated exactly like the sample filters, except that no air was drawn through the filter. After collection, the filters were immediately removed from the sampler, packed in pre-baked aluminum foils (450 °C for 3 h), sealed in polyethylene bags and stored in a freezer at -18 °C until analysis.

2.2 Thermal/optical organic carbon (OC) and elemental carbon (EC) analysis

Filter pieces of 1.5 cm^2 were taken for OC and EC analysis using a carbon analyzer (Model 5L, Sunset Laboratory, Inc., Portland, OR, USA) following the thermal-optical transmittance protocol EUSAAR_2 (Cavalli et al., 2010). In the EUSAAR_2 protocol the filter sample is heated stepwise in an inert helium (He) atmosphere up to 650 °C to thermally desorb organic compounds. After a rapid cooling to 500 °C the sample is heated again stepwise up to 850 °C in an oxidizing 98% He/2% O_2 atmosphere to oxidize EC. All carbon gases are converted to CO_2 and detected with a non-dispersive infrared (NDIR) detector. During heating in the inert He atmosphere, a fraction of OC pyrolyzes (chars) to light-absorbing EC, as demonstrated by decreasing transmission signal. When the charred OC and original EC are released in the He/O_2 atmosphere, transmission signal increases again. The split between OC and EC is set when the transmission signal reaches their pre-pyrolysis value. The sum of OC and EC is total carbon (TC).

At the beginning of each work day, the instrument is calibrated using a sucrose standard solution. The instrument blank, representing the background contamination of the instrument during the analysis, is measured every day and negligible (TC < 0.2 μg cm^{-2}) compared to the TC loading of the samples (13–246 μg cm^{-2}; range). The reproducibility determined by duplicate analysis of the filter samples was within 6% for OC and 5% for EC. The average field blank of OC was 0.9 ± 0.2 μg cm^{-2} (N=6, equivalent to ~ 0.23 ± 0.05 μg m^{-3}), which was subtracted from the sample OC concentrations. EC on field blanks was in most cases below the detection level. Details of the OC/EC measurement can also be found in Zenker et al. (2017).

2.3 Stable carbon isotopic composition of EC

The stable carbon isotopic composition of EC was measured at the Stable Isotope Laboratory at the Institute of Earth Environment, Chinese Academy of Sciences. To remove OC, filter pieces were heated at 375 °C for 3 h in a vacuum-sealed quartz tube in the presence of CuO catalyst grains. Extraction of EC was done by heating the carbon that remained on the filters at 850 °C for 5 h in another vacuum-sealed quartz tube. The resulting CO_2 from EC was isolated by a series of cold traps and quantified manometrically. The stable carbon isotopic composition of the purified CO_2 was determined as $\delta^{13}C$ ($\delta^{13}C_{EC}$ for EC) by offline analysis with a Finnigan MAT-251 mass spectrometer (Bremen, Germany). $\delta^{13}C$ values are expressed in the delta notation as per mil (‰) deviation from the international standard Vienna Pee Dee Belemnite (V-PDB):

$$\delta^{13}C\ (‰) = \left[\frac{(^{13}C/^{12}C)_{sample}}{(^{13}C/^{12}C)_{V-PDB}} - 1\right] \times 1000. \tag{1}$$

A routine laboratory working standard with a known $\delta^{13}C$ value was measured every day. The analytical precision of $\delta^{13}C$ was better than $\pm$ 0.3 ‰ based on duplicate analyses. Details of stable carbon isotope measurements are described in our previous studies (Cao et al., 2011, 2013; Ni et al., 2018).

Pyrolyzed OC can be formed through charring during the OC removal procedure and is released at the high temperature of EC step. To assess the potential effect of pyrolyzed OC on the measured $\delta^{13}C_{EC}$, we conducted a sensitivity analysis based on isotope mass balance (See details in the Supplemental S1). This analysis shows that even for high contribution from pyrolyzed OC to the isolated EC of 20%, the expected difference in $\delta^{13}C$ between measured EC and true EC is <1‰.

2.4 Radiocarbon (^{14}C) measurements of OC, WIOC and EC

2.4.1 Sample selection for ^{14}C analysis

For ^{14}C analysis of OC, WIOC and EC, 3 composite samples per season were selected to represent high (H), medium (M) and low (L) concentrations of total carbon (TC = OC + EC), to cover various pollution conditions in each season. Each composite sample consists of 2 to 4 24 h filter pieces with similar TC loadings and air mass backward trajectories (Fig. S1, Table S1). In total, 36 radiocarbon data were measured, including 12 OC, 12 WIOC and 12 EC. ^{14}C values of WSOC are calculated from ^{14}C values of OC and WIOC according to the isotope mass balance (Eq. 4).

2.4.2 Extraction of OC, WIOC and EC

OC, WIOC and EC extractions were conducted on our custom-built aerosol combustion system (ACS). The ACS has been described in detail by Dusek et al. (2014) and evaluated in two intercomparison studies (Szidat et al., 2013; Zenker et al., 2017). In brief, the ACS consists of a reaction tube and a CO_2 purification line. In the reaction tube aerosol filter samples are inserted into a filter holder and heated at different temperatures in pure O_2. Combustion products are fully oxidized using a platinum catalyst. The resulting CO_2 is separated from other gases (e.g., NO_x, water vapor) in the purification line. Here, NO_x and liberated halogens are first removed by a heated oven (650 °C) filled with copper grains and silver, water is then removed by a U-type tube cooled with dry ice-ethanol mixture (around -70 °C) and a flask containing phosphorus pentoxide (P_2O_5). The amount of purified CO_2 is determined manometrically in a calibrated volume and CO_2 is subsequently stored in flame-sealed glass ampoules.

OC is combusted by heating filter pieces at 375 °C for 10 min. WIOC and EC are combusted from water-extracted filter pieces. By water-extraction, water-soluble OC (WSOC) is removed from filter pieces (Zhang et al., 2012; Bernardoni et al., 2013; Dusek et al., 2014). For WIOC, a water-extracted filter piece is heated at 375 °C for 10 minutes. Subsequently, the oven temperature is increased to 450 °C for 3 min to remove the most refractory OC that left on the filter. However, during this step some less refractory EC might be lost. After this step, OC has been completely removed from the filter pieces. Finally, the remaining EC is combusted by heating the filter at 650 °C in O_2 for 5 min (Dusek et al., 2017; Zenker et al.,

2017). EC recovery after the intermediate 450 °C step was approximately 70%, estimated by comparing to the EC quantified by EUSAAR_2 protocol.

Contamination during the extraction procedure is determined by following the same extraction procedures with either empty filter boat or pre-heated filters (at 650 °C in O_2 for 10 min). The contamination yields on average 0.85 µgC OC, 0.73 µgC WIOC and 0.72 µgC EC per extraction, respectively. Compared with our sample size of 45–210 µgC OC, 45–328 µgC WIOC and 15–184 µgC EC, the contamination is relatively small (<5 % of the sample amount).

2.4.3 ^{14}C measurements by accelerator mass spectrometer (AMS)

[14]C measurements were conducted using the the Mini Carbon Dating System (MICADAS) AMS at the Centre for Isotope Research at the University of Groningen. The extracted CO_2 is released from the glass ampules and captured by a zeolite trap within a gas inlet system (Ruff et al., 2007), where the sample is diluted using He to 5% CO_2 (Salazar et al., 2015). The CO_2/He mixture is directly introduced into the Cs sputter ion sources of the MICADAS at a constant rate (Synal et al., 2007).

The ^{14}C/^{12}C ratio of an aerosol sample is usually normalized to the ^{14}C/^{12}C ratio of an oxalic acid standard (OXII) and expressed as fraction modern ($F^{14}C$). Following the definition of fraction modern (Mook and van der Plicht, 1999; Reimer et al., 2004), the ^{14}C/^{12}C ratio of OXII is related to the unperturbed atmosphere in the reference year of 1950 by multiplying it with a factor of 0.7459:

$$F^{14}C = \frac{(^{14}C/^{12}C)_{sample,[-25]}}{0.7459 \times (^{14}C/^{12}C)_{OXII,[-25]}} \tag{2}$$

where the ^{14}C/^{12}C ratio of the sample and OXII are both corrected for machine background and normalized to $\delta^{13}C = -25$ ‰ with respect to V-PDB to correct for isotope fractionation. $\delta^{13}C = -25$ ‰ is the postulated mean value of terrestrial wood (Stuiver and Polach, 1977).

The $F^{14}C$ values are corrected for memory effect (Wacker et al., 2010) using alternate measurements of OXII and ^{14}C-free material as gaseous standards. Correction for instrument background (Salazar et al., 2015) is done by subtracting the memory corrected $F^{14}C$ values of the ^{14}C-free standard. Finally, the values are normalized to the average value of the (memory and background corrected) OXII standards. A set of secondary standards is used to assess the robustness and reliability of the data. This includes IAEA-C7 with a consensus value of $F^{14}C = 0.4953 \pm 0.0012$ and sample masses of 76 µg and 80 µg and IAEA-C8 with a consensus value of $F^{14}C = 0.1503 \pm 0.0017$ and sample masses of 63 µg and 100 µg. All standards including OXII and ^{14}C-free material used for data correction and IAEA-C7 and IAEA-C8 for quality control of AMS measurements are measured on the same day as the samples. $F^{14}C$ values of secondary standards undergo the same data correction as the samples. Results of IAEA-C7 and C8 agree within uncertainties (Table S2).

$F^{14}C$ of carbon from fossil sources is 0, and carbon from non-fossil sources (or "contemporary" sources) should have $F^{14}C$ of 1. But the extensive release of ^{14}C from nuclear bomb tests in the late 1950s and early 1960s and ^{14}C-free CO_2 from fossil fuel combustion has perturbed the atmospheric $F^{14}C$ values significantly. The former increased the $F^{14}C$ in the atmosphere by up to a factor of 2 in the northern hemisphere in the 1960s. The nuclear tests have been banned in the atmosphere, outer space and under water since 1963. Since then, the atmospheric $F^{14}C$ has been slowly decreasing, as ^{14}C is mainly taken up by the oceans and terrestrial biosphere and diluted by ^{14}C-free CO_2 (Hua and Barbetti, 2004; Levin et al., 2010).In 2010, the $F^{14}C$ of the atmospheric CO_2 is approximately 1.04 (Levin et al., 2008, 2010), whereas in 2014 it decreased to 1.02 (Vlachou et al., 2018).

2.5 Estimation of source contributions to different carbon fractions

$F^{14}C$ of EC, OC and WIOC (i.e., $F^{14}C_{(EC)}$, $F^{14}C_{(OC)}$ and $F^{14}C_{(WIOC)}$, respectively) are directly measured. Mass concentrations (M_{WSOC}) and $F^{14}C$ of WSOC ($F^{14}C_{(WSOC)}$) can be calculated as

$$M_{WSOC} = M_{OC} - M_{WIOC} \tag{3}$$

$$F^{14}C_{(WSOC)} = \frac{F^{14}C_{(OC)} \times M_{OC} - F^{14}C_{(WIOC)} \times M_{WIOC}}{M_{OC} - M_{WIOC}}. \tag{4}$$

where M_{OC} and M_{WIOC} are mass concentrations of OC and WIOC, respectively. M_{OC} is measured by the thermal-optical method as described in Sect. 2.2.

To estimate M_{WIOC}, we assume two extreme cases following the method of Dusek et al. (2017). (1) WIOC is completely recovered. That is, the recovery of WIOC is 100%, where the recovery is estimated by dividing the WIOC mass extracted using ACS ($M_{WIOC,e}$) with the WIOC mass in the aerosol samples. But the WIOC combustion temperature of 375 °C in the ACS is highly likely not high enough to recover 100 % of WIOC. Thus, this estimation is an underestimate of M_{WIOC} ($M1_{WIOC}$). (2) We assume that WIOC has the same recovery as OC. The M_{WIOC} can be calculated by dividing $M_{WIOC,e}$ by the OC recovery. Due to the fact that usually less WIOC than OC is lost to charring, this probably is an overestimate of M_{WIOC} ($M2_{WIOC}$). M_{WIOC} is assumed to vary from $M1_{WIOC}$ to $M2_{WIOC}$. The most likely value of M_{WIOC} is chosen at $M1_{WIOC}+2/3\times(M2_{WIOC}-M1_{WIOC})$, because it is more likely that WIOC has a similar recovery as OC rather than 100 % recovery. Once M_{WIOC} is estimated, the $F^{14}C_{(WSOC)}$ can be calculated following the Eq. (4). The best estimate and ranges of $F^{14}C_{(WSOC)}$ is presented in Fig. S2 and Table S1. $F^{14}C_{(WSOC)}$ is only slightly sensitive to M_{WIOC}. If we shift the M_{WIOC} from $M1_{WIOC}$ to $M2_{WIOC}$, the average values of $F^{14}C_{(WSOC)}$ only change by less than 0.03 (absolute differences).

$F^{14}C_{(EC)}$ can be converted to the relative contribution of biomass burning to EC ($f_{bb}(EC)$) by dividing with $F^{14}C$ of biomass burning ($F^{14}C_{bb} = 1.10 \pm 0.05$; Lewis et al., 2004; Mohn et al., 2008; Palstra and Meijer, 2014), to eliminate the effect from nuclear bomb tests in the 1960s. $F^{14}C_{bb}$ represents $F^{14}C$ of biomass burning including wood burning and crop residue

burning. This is because that biomass burning in Xi'an mainly includes household usage of wood and crop residues as well as open burning of crop residues. $F^{14}C$ for burning of annual crop has a similar value of current atmospheric CO_2. $F^{14}C$ of wood burning is higher than that and varies with the age of tree. Estimates of $F^{14}C$ for wood burning are based on tree-growth models (e.g., Lewis et al., 2004; Mohn et al., 2008) and found to range from 1.08 to 1.30 relating to wood age and fell date (Heal, 2014, and references therein). The lower limit of $F^{14}C_{bb}$ corresponds to burning of young wood (5–10 years old tree harvested between 2010 and 2015) and crop residues as main sources of EC, and the upper end of $F^{14}C_{bb}$ corresponds to older wood (30–60 years old tree) combustion as the main source of EC.

Analogously, the relative contribution of non-fossil sources to OC, WIOC and WSOC (i.e., $f_{nf}(OC)$, $f_{nf}(WIOC)$ and $f_{nf}(WSOC)$, respectively) can be estimated from their corresponding $F^{14}C$ values and $F^{14}C_{nf}$. $F^{14}C_{nf}$ is $F^{14}C$ of non-fossil sources include both biomass burning and biogenic emissions. $F^{14}C$ of biogenic sources can be estimated from long-term $^{14}CO_2$ measurements at the Schauinsland background station (Levin and Hammer, 2013; Levin et al., 2010). In Xi'an, biogenic OC is probably not very important, as could be expected from high concentrations of carbonaceous aerosols and strong anthropogenic sources. $F^{14}C_{nf}$ is thus estimated as 1.09 ± 0.05 (Lewis et al., 2004; Levin et al., 2010; Y. L. Zhang et al., 2014). The central value of 1.09 corresponds to 15% contribution of biogenic OC to OC.

EC is primarily produced from biomass burning (EC_{bb}) and fossil fuel combustion (EC_{fossil}), and absolute EC concentrations from each source can be estimated as:

$$EC_{bb} = M_{EC} \times f_{bb}(EC) \qquad (5)$$

$$EC_{fossil} = M_{EC} \times \left(1 - f_{bb}(EC)\right) = M_{EC} \times f_{fossil}(EC) \qquad (6)$$

where $f_{fossil}(EC)$ is the relative contribution of fossil sources to EC, M_{EC} are mass concentrations of EC. Analogously, mass concentrations of OC, WIOC and WSOC from non-fossil sources (OC_{nf}, $WIOC_{nf}$ and $WSOC_{nf}$, respectively) and fossil sources (OC_{fossil}, $WIOC_{fossil}$ and $WSOC_{fossil}$, respectively) can be determined.

More detailed source apportionment of OC can be achieved by combining ^{14}C-apportioned OC and EC with characteristic primary OC/EC ratios for each source (i.e., using EC as a tracer of primary emissions; EC tracer method). Biomass burning usually has higher primary OC/EC ratios ($r_{bb} = 3–10$) than those for coal combustion ($r_{coal} = 1.6–3$) and vehicle exhausts ($r_{vehicle} = 0.5–1.3$) (Ni et al. (2017) and references therein). Best estimate of r_{bb} (4 ± 1; average $\pm$ SD), r_{coal} (2.38 ± 0.44), and $r_{vehicle}$ (0.85 ± 0.16) is done through a literature search as described in Ni et al. (2018) and comparable to values used in ealier ^{14}C source apportionment in China (Y. L. Zhang et al., 2014, 2015a).

Primary biomass burning OC (POC_{bb}) can be estimated by multiplying EC_{bb} with r_{bb}:

$$POC_{bb} = EC_{bb} \times r_{bb} \qquad (7)$$

Other non-fossil OC excluding POC_{bb} ($OC_{o,nf}$) can be estimated as:

$$OC_{o,nf} = OC_{nf} - POC_{bb} \tag{8}$$

where $OC_{o,nf}$ includes OC from all non-fossil sources other than primary biomass burning, thus mainly consists of secondary OC from biomass burning (SOC_{bb}), primary and secondary biogenic OC, as well as cooking emissions. In most cases, contributions of primary biogenic OC to $PM_{2.5}$ are likely small (Gelencsér et al., 2007; Guo et al., 2012).

OC_{fossil} includes both primary and secondary OC from fossil sources (POC_{fossil} and SOC_{fossil}, respectively):

$$OC_{fossil} = POC_{fossil} + SOC_{fossil}, \tag{9}$$

where POC_{fossil} can be estimated from EC_{fossil} and primary OC/EC ratio of fossil fuel combustion (r_{fossil}):

$$POC_{fossil} = EC_{fossil} \times r_{fossil}. \tag{10}$$

Fossil sources in China are almost exclusively from coal combustion and vehicle emissions, thus r_{fossil} can be estimated as

$$r_{fossil} = r_{coal} \times p + r_{vehicle} \times (1-p), \tag{11}$$

where p is the relative contribution of coal combustion to fossil EC. That is, $p = EC_{coal}/EC_{fossil}$, where estimation of EC_{coal} is achieved by combining $F^{14}C_{(EC)}$ and $\delta^{13}C_{EC}$ with the Bayesian calculations as described in details in the Sect. 2.6 and Supplement S2.

To propagate uncertainties, a Monte Carlo simulation with 10000 individual calculations was conducted. For each individual calculation, $F^{14}C_{(EC)}$, $F^{14}C_{(OC)}$, $F^{14}C_{(WIOC)}$ and concentrations of EC, OC and WIOC are randomly chosen from a normal distribution symmetric around the measured values with the experimental uncertainties as standard deviation (SD). For $F^{14}C_{bb}$, $F^{14}C_{nf}$, r_{bb}, r_{coal} and $r_{vehicle}$ random values are chosen from a triangular frequency distribution with its maximum at the central value and is 0 at the lower limit and upper limit. For p values, random values from the respective probability density function (PDF) of p were used (Supplement S1). In this way 10000 random sets of variables can be generated. For $f_{bb}(EC)$, $f_{nf}(OC)$, $f_{nf}(WIOC)$, $f_{nf}(WSOC)$, EC_{bb}, EC_{fossil}, OC_{nf}, OC_{fossil}, $WIOC_{nf}$, $WIOC_{fossil}$, $WSOC_{nf}$, $WSOC_{fossil}$, POC_{bb} and $OC_{o,nf}$, the derived average represents the best estimate, and the SD represents the combined uncertainties (Tables 1, S4). For POC_{fossil} and SOC_{fossil}, the median value is considered as the best estimates and the interquartile range (25th–75th percentile) are used as uncertainties, because the PDFs of POC_{fossil} and SOC_{fossil} are asymmetric (Fig. S3b, Table S4).

2.6 Source apportionment of EC using Bayesian statistics

Using $F^{14}C$ and $\delta^{13}C$ signatures of EC ($F^{14}C_{(EC)}$, $\delta^{13}C_{EC}$) and assuming isotope mass balance in combination with a Bayesian Markov chain Monte Carlo (MCMC) scheme, it is possible to differentiate the 3 main sources of EC: biomass burning, liquid fossil fuel combustion (i.e., vehicle emissions) and coal combustion (Andersson et al., 2015; Li et al., 2016; Winiger et

al., 2016; Fang et al., 2018). EC from fossil sources can be first separated from biomass burning by $F^{14}C_{(EC)}$. Further, $\delta^{13}C_{EC}$ allows separation of fossil sources into coal and liquid fossil fuel burning:

$$\begin{pmatrix} F^{14}C_{(EC)} \\ \delta^{13}C_{EC} \\ 1 \end{pmatrix} = \begin{pmatrix} F^{14}C_{bb} & F^{14}C_{liq.fossil} & F^{14}C_{coal} \\ \delta^{13}C_{bb} & \delta^{13}C_{liq.fossil} & \delta^{13}C_{coal} \\ 1 & 1 & 1 \end{pmatrix} \begin{pmatrix} f_{bb} \\ f_{liq.fossil} \\ f_{coal} \end{pmatrix} \tag{12}$$

where the last row ensures the mass balance; f_{bb}, $f_{liq.fossil}$ and f_{coal} are the relative contribution from biomass burning, liquid fossil fuel combustion and coal combustion to EC, respectively; $F^{14}C_{bb}$ is the $F^{14}C$ of biomass burning (1.10 ± 0.05), as mentioned in Sect. 2.5. $F^{14}C_{liq.fossil}$ and $F^{14}C_{coal}$ are zero due to the long-time decay. $\delta^{13}C_{bb}$, $\delta^{13}C_{liq.fossil}$ and $\delta^{13}C_{coal}$ are the $\delta^{13}C$ signature of EC emitted from biomass burning, liquid fossil fuel combustion and coal combustion, respectively. The means and the standard deviations for $\delta^{13}C_{bb}$ (-26.7 $\pm$ 1.8 ‰ for C3 plants, and -16.4 $\pm$ 1.4 ‰ for corn stalk), $\delta^{13}C_{liq.fossil}$ (-25.5 $\pm$ 1.3 ‰), and $\delta^{13}C_{coal}$ (-23.4 $\pm$ 1.3 ‰) are compiled and established by literature studies in previous publications (Andersson et al. (2015) and references therein; Ni et al., 2018). The source endmembers for $\delta^{13}C$ are less well-constrained than for $F^{14}C$, as $\delta^{13}C$ varies with fuel types and burning conditions. For example, the range of possible $\delta^{13}C_{liq.fossil}$ overlaps to a small extent with the range of $\delta^{13}C_{coal}$, although liquid fossil fuels are usually more depleted than coal. The MCMC technique takes into account the variability in the source signatures of $F^{14}C$ and $\delta^{13}C$ (Parnell et al., 2010, 2013), where $\delta^{13}C$ introduces a larger uncertainty than $F^{14}C$. Uncertainties of $\delta^{13}C_{bb}$, $\delta^{13}C_{liq.fossil}$, $\delta^{13}C_{coal}$ and $F^{14}C_{bb}$ as well as the measured ambient $\delta^{13}C_{EC}$ and $F^{14}C_{(EC)}$ are propagated. The results of the MCMC calculations are the posterior PDFs for f_{bb}, $f_{liq.fossil}$ and f_{coal}. The PDFs of $f_{liq.fossil}$ and f_{coal} are skewed. By contrast, the PDFs of f_{bb} is symmetric as it is well-constrained by $F^{14}C$ (Fig. 6). In this study, the median is used to represent the best estimate of the f_{bb}, $f_{liq.fossil}$ and f_{coal}. Uncertainties of this best estimate are expressed as an interquartile range (25th-75th percentile) of the corresponding PDFs. The MCMC-derived f_{bb} (calculated by Eq. 12) is very similar to that obtained directly from radiocarbon data ($f_{bb}(EC)$, Eq. 5) as both of them are well constrained by $F^{14}C$. In this study, f_{bb} and $f_{bb}(EC)$ are therefore used interchangeably. Details on the MCMC-driven Bayesian approach have been described in our earlier study (Ni et al., 2018).

3 Results

3.1 ^{14}C-based source apportionment of EC and OC

EC is derived mainly from fossil sources, regardless of differences in EC concentrations and seasonal variations. The relative contribution of fossil fuel combustion to EC ($f_{fossil}(EC)$) ranges from 69% to 89%, with an annual average of 82 $\pm$ 6% (Fig. 1a). The relative contribution of fossil sources to OC ($f_{fossil}(OC)$ is consistently smaller than $f_{fossil}(EC)$ (Fig. 1b). The values of $f_{fossil}(OC)$ range from 41% to 51%, with an annual average of 47 $\pm$ 4%. The absolute difference in the fossil fractions between OC and EC is on average 35% (28%–42%; range). The main reason for this difference is that biomass burning emits more OC relative to EC compared to the fossil sources (Streets et al., 2003; Akagi et al., 2011; Zhou et al., 2017). Thus,

even if biomass burning contributes a small fraction to EC, it will have a much higher contribution to primary OC. Additionally other non-fossil sources, such as secondary biomass burning emissions, primary and secondary biogenic emissions as well as cooking contribute to OC, but not to EC.

The annual average f_{fossil}(EC) and f_{fossil}(OC) reported here is consistent with the results reported at an urban site of the same Chinese city in 2008/2009 (f_{fossil}(EC) = 83 ± 5%, f_{fossil}(OC) = 46 ± 8%; Ni et al., 2018), an urban site of Beijing, China in 2013/2014 (f_{fossil}(EC) = 82 ± 7%, f_{fossil}(OC) = 48 ± 12%; Zhang et al., 2017) and 2010/2011 (f_{fossil}(EC) = 79 ± 6%; Zhang et al., 2015b) and a background receptor site of Ningbo, China (f_{fossil}(EC) = 77 ± 15%; Liu et al., 2013). Much lower f_{fossil}(EC) and f_{fossil}(OC) was found at a regional background site in South China in 2005/2006 (f_{fossil}(EC) = 38 ± 11% and f_{fossil}(OC) = 19 ± 10% for Hainan; Y. L. Zhang et al., 2014), regional receptor sites in South Asia in 2008/2009 (f_{fossil}(EC) = 27 ± 6% and f_{fossil}(OC) = 31 ± 5% for Hanimaadhoo, Maldives and f_{fossil}(EC) = 41 ± 5% and f_{fossil}(OC) = 36 ± 5% for Sinhagad, India; Sheesley et al., 2012), where regional/local biomass burning contributes much more to carbonaceous aerosols than fossil fuel combustion and the ^{14}C levels can change significantly with the origin of air masses.

The f_{fossil}(EC) and f_{fossil}(OC) follow the same seasonal trends: the values are lower in winter and higher in the rest of the seasons (i.e., warm period). Within the warm period, both are slightly higher in spring (f_{fossil}(EC) = 86 ± 3%, f_{fossil}(OC) = 50 ± 1%) than in summer and autumn (f_{fossil}(EC) = 84 ± 2%, f_{fossil}(OC) = 47 ± 3%) in general and also to be slightly lower under the cleanest periods (i.e., in spring, summer and autumn, f_{fossil}(EC) and f_{fossil}(OC) in polluted days ("H" and "M" samples) were higher than in clean days ("L" samples); Fig. 1, Tables 1, S5). The low f_{fossil}(EC) in winter is due to the substantially increased contribution from biomass burning (mainly wood burning) for heating in winter, which gradually stops in spring but in summer and early autumn, open biomass burning (mainly crop residues) occurs in Xi'an and its surrounding areas. Some biomass burning for cooking is probably present all year round (Huang et al., 2012; T. Zhang et al., 2014). The seasonality in biomass burning activity is consistent with the variations of f_{bb}(EC). f_{bb}(EC) is higher in winter (28 ± 4%) than that in other seasons (i.e., warm period, on average 15 ± 2 %). This is in line with our previous study in Xi'an, China in 2008/2009 (Ni et al., 2018). By comparison with literature data for Beijing, Beijing shows a very different seasonal trend, where f_{bb}(EC) was lowest in summer (~7%) and increased to ~20% during the rest of the year (Zhang et al., 2017). The distinct different values and seasonality of f_{bb}(EC) in Xi'an and Beijing indicate that biomass burning emissions are seasonally dependent and their influences vary spatially in different Chinese cities. The seasonal trends of f_{fossil}(OC) were different in Beijing as well, with higher f_{fossil}(OC) in winter than in other seasons (Yan et al., 2017; Zhang et al., 2017). This is in line with previous source apportionment results that during wintertime biomass burning is a major source of OC in Xi'an and coal combustion is a dominant source for OC in Beijing (R. J. Huang et al., 2014; Elser et al., 2016).

EC concentrations from fossil fuel combustion (EC$_{fossil}$) span a range from about 0.6 to 7 µg m^{-3} and increase by roughly a factor of 3 from summer to winter when separately comparing clean and polluted periods. The remaining EC is contributed by biomass burning (EC$_{bb}$), which varies in a wider range than EC$_{fossil}$ from about 0.1 to 3 µg m^{-3} (Fig. 1a, Table S3). EC$_{fossil}$

values are on average 2–3 times higher than EC_{bb} in winter and 5–8 times higher in other seasons. This implies that the winter-summer differences in biomass burning emissions is larger than fossil fuel combustion emissions, regardless of the fact that both biomass burning and coal combustion are expected to increase during wintertime for heating (T. Zhang et al., 2014; Shen et al., 2017; Zhu et al., 2017). OC concentrations from fossil fuel combustion (OC_{fossil}) range from about 1 to 20 µg m^{-3}, with an average of 6.8 µg m^{-3}, which is comparable to non-fossil OC concentrations (range: 2–28 µg m^{-3}; mean: 8.2 µg m^{-3}). Clear seasonal variations were observed in both EC and OC from fossil and non-fossil sources, with maxima in winter and minima in summer (Table S6). This is mainly because of an increase in coal burning and biomass burning for heating as well as unfavorable meteorological conditions in winter.

3.2 ^{14}C- based source apportionment of water-soluble and water-insoluble OC

The fossil contribution to total WIOC (f_{fossil}(WIOC)) varied from 49 ± 1% in winter to 60 ± 5% in summer, with an annual average of 55 ± 5%. In winter the enhanced biomass burning is a source of non-fossil WIOC (Dusek et al., 2017). The relative contributions of fossil sources to WSOC (f_{fossil}(WSOC) = 42 ± 6%) were smaller than that to WIOC for nearly all the samples throughout the year. In winter both primary emission and secondary formation from biomass burning contribute to WSOC and in the warm period additionally biogenic SOC, though the latter concentrations are probably relatively low. In addition, primary fossil emissions are expected to contribute very little to WSOC, so the lower fossil fractions in WSOC are in line with expectations. In this study, the largest differences between fossil fractions in WIOC and WSOC were found to be 36% for sample Summer-L (e.g., low TC concentrations in summer). Summer-L had the lowest f_{fossil}(WSOC) of 28 ± 2% (Fig. 2a), which was contrary to the stable f_{fossil}(EC) in the warm period (Fig. 1a) and therefore cannot be explained by an increase in primary (or probably secondary) biomass burning OC. This indicates that the lowest f_{fossil}(WSOC) for Summer-L was probably due to the impact of biogenic OC in the clean period.

WSOC concentrations from non-fossil sources ($WSOC_{nf}$) are larger than WSOC from fossil sources ($WSOC_{fossil}$) at 95% confidence level (paired t-test, P-value=0.016), with an average of 5.1 µg m^{-3} (range of 1.5–16.7 µg m^{-3}) for $WSOC_{nf}$ versus an average of 3.6 µg m^{-3} (range of 0.6–9.4 µg m^{-3}) for $WSOC_{fossil}$ (Fig. 2). WIOC concentrations from non-fossil sources ($WIOC_{nf}$) do not differ significantly from fossil sources ($WIOC_{fossil}$) (paired t-test, P-value=0.113). $WSOC_{nf}$, $WSOC_{fossil}$, $WIOC_{nf}$ and $WIOC_{fossil}$ show the same seasonal trends, with higher mass concentrations in winter and lower in the warm period. $WSOC_{nf}$ is responsible for ~ 35% of the increased OC mass in winter, followed by $WIOC_{nf}$ (~24%), $WIOC_{fossil}$ (~ 22%) and $WSOC_{ff}$ (~ 19%).

Figure 2b shows the fraction of $WIOC_{nf}$, $WSOC_{nf}$, $WIOC_{fossil}$ and $WSOC_{fossil}$ in the total OC in different seasons. WSOC (the sum of the blue areas) on yearly average accounted for 60 ± 5% of OC (ranging from 53–70%), consistent with previous measurements in Xi'an (Cheng et al., 2013; Zhang et al., 2018; Zhao et al., 2018). The remaining 40 ± 5% of OC is WIOC (the sum of red areas). Throughout the year, $WSOC_{nf}$ was the largest contributor to OC, which accounts for about one-third

of the total OC, probably resulting from the mostly water-soluble biomass-burning POC and SOC as well as biogenic SOC (e.g., Mayol-Bracero et al., 2002; Nozière et al., 2015; Dusek et al., 2017).The respective proportions of $WSOC_{fossil}$, $WIOC_{fossil}$ and $WIOC_{nf}$ in OC were 26 %, 21% and 17% on a yearly average in descending order, very likely related to secondary fossil OC, primary fossil OC and primary biomass burning, respectively (Weber et al., 2007; Dai et al., 2015; Dusek et al., 2017; Yan et al., 2017).

The majority (60–76%) of the non-fossil OC was water-soluble. This result is qualitatively consistent with findings reported for an urban site of Xi'an (Zhang et al., 2018) and other places such as at an urban site of Beijing, China (Zhang et al., 2018), an urban or rural site in Switzerland (Zhang et al., 2013), a remote site on Hainan Island, southern China (Y. L. Zhang et al., 2014) and two rural sites in the eastern United States (Wozniak et al., 2012) and a regional background site in the Netherlands (Dusek et al., 2017). Seasonal variations of $(WSOC/OC)_{nf}$ ratios were also observed, with lower ratios in winter (around 0.6) and higher ratios in summer and spring (around 0.7). This reflects the higher fraction of $WIOC_{nf}$ in OC_{nf} during wintertime, resulting from primary biomass burning emissions (Dusek et al., 2017). In summer and spring, concentrations of $WSOC_{nf}$ and OC_{nf} are both small and the contribution of biogenic SOC to $WSOC_{nf}$ can be noticeable (Dusek et al., 2017).

The fossil OC is less water soluble in winter with somewhat lower $(WSOC/OC)_{fossil}$ ratios than in the rest of seasons (i.e., warm period). $(WSOC/OC)_{fossil}$ ratios in winter (0.50 ± 0.03, with a range of 0.48–0.53) fall into the lower end of the range of $(WSOC/OC)_{fossil}$ ratios in warm period (0.57 ± 0.08, with a range of 0.42–0.70; Fig. 3). $WSOC_{fossil}$ can come mainly from secondary formation and/or photochemical aging of primary organic aerosols, thus the higher $(WSOC/OC)_{fossil}$ ratios in the warm period suggest an enhanced SOC formation from fossil VOCs from vehicle emissions and/or coal burning. In spring and summer there is a clear increasing tend of $(WSOC/OC)_{fossil}$ in more polluted periods. Elevated $(WSOC/OC)_{fossil}$ ratios in polluted periods are very likely related to the formation of high pollutant concentrations in spring and summer. More stagnant conditions in the polluted periods (indicated by lower wind speed, see Fig. 3) that allow for accumulation of pollutants also provide more time for photochemical processes and SOC formation. As a consequence, formation of fossil WSOC will increase in stagnant conditions. At the same time, $(WIOC/EC)_{fossil}$ ratios decline when pollution gets worse, suggesting removal of WIOC, likely through photochemical reactions. This can shift the water-soluble vs. water-insoluble distribution for fossil OC to WSOC (Szidat et al., 2009). As a consequence, the $(WSOC/OC)_{fossil}$ ratio is higher for Summer-H (0.62) than for Summer-L (0.42).

3.3 Combustion sources apportioned by stable carbon isotopes

Along with radiocarbon data, the stable carbon isotopic ratio of EC (denoted by $\delta^{13}C_{EC}$) provides additional insight into source apportionment of EC, especially between different type of fossil sources (i.e., coal versus liquid fossil fuel combustion). Figure 4 shows ^{14}C-based f_{fossil}(EC) against $\delta^{13}C_{EC}$ in Xi'an in different seasons for 2015/2016 from this study and in winter for 2008/2009 from Ni et al. (2018), together with the ranges of endmembers (i.e., isotopic signature) for the

different EC sources of coal combustion, liquid fossil fuel combustion and biomass burning (C3 and C4 plants). f_{fossil}(EC) is well constrained by $F^{14}C_{(EC)}$, clearly separating fossil sources from biomass burning. In contrast to ^{14}C, the source endmembers (i.e., isotopic signature) for $\delta^{13}C$ are less well constrained and $\delta^{13}C$ values for liquid fossil fuel combustion overlap with $\delta^{13}C$ values for both coal and C3 plant combustion. Regardless of the changes of $\delta^{13}C_{EC}$ in different seasons, all the $\delta^{13}C_{EC}$ data points fall within the range of burning C3 plant, coal and liquid fossil fuel, indicating that C3 plant is the dominating biomass type in Xi'an with little influence from C4 plant burning. In Xi'an, the dominant C4 plant is corn stalk, which is burned for cooking and heating in the areas surrounding Xi'an (Sun et al., 2017; Zhu et al., 2017).

The annually averaged $\delta^{13}C_{EC}$ is -24.9 ± 0.4 ‰ (± SD). Moderate seasonal variation of $\delta^{13}C_{EC}$ was observed, reflecting a moderate shift in the relative contributions from combustion sources throughout the year. The $\delta^{13}C_{EC}$ in autumn (-25.3 ± 0.2 ‰) and summer (-25.0 ± 0.3 ‰) are most depleted and fall into the overlapped $\delta^{13}C$ range for liquid fossil fuel combustion and C3 plant burning. Because the ^{14}C values in autumn and summer indicate that biomass burning contribution to EC is relatively low (~16%), we can expect that liquid fossil fuel combustion dominates EC in autumn and summer. $\delta^{13}C_{EC}$ signatures in winter (-24.8 ± 0.2 ‰) scatter into the range for C3 plant, liquid fossil fuel and coal combustion, implying that EC is influenced by mixed sources. The $\delta^{13}C_{EC}$ signatures in spring (-24.6 ± 0.3 ‰) overlaps with both liquid fossil fuel combustion and coal combustion. Only the sample Spring-L is characterized by the most enriched $\delta^{13}C_{EC}$ value among all the samples, even more enriched than wintertime $\delta^{13}C_{EC,}$ when coal combustion for heating is expected to influence EC strongly. At the same time, higher contributions from biomass burning (i.e., lower f_{fossil}(EC)) were observed for Spring-L. This suggests contributions from a ^{13}C-enriched biomass burning, that is, corn stalk burning (C4 plant). The contribution of this regional source can become noticeable in the relatively clean air that characterizes Spring-L.

To estimate seasonal source contributions to EC, we combined all the data points from each season for the Bayesian Markov chain Monte Carlo techniques (MCMC) calculations. The MCMC results (Figs. 5, 6) show that the dominant EC source is liquid fossil fuel combustion (i.e., vehicle emissions). Liquid fossil fuel combustion accounts for 64 % (median; 45–74%, interquartile range) of EC in autumn, 60% (41–72%) in summer, 53% (33–69%) in spring, and 46% (29–59%) in winter, respectively, in descending order. Biomass burning EC is a small fraction of total EC throughout the year. However, the relative contribution of biomass burning to EC increased in winter (28 %; 26–31%), and is comparable to the relative contribution of coal combustion (25%; 13–41%). In the warm period, coal combustion for cooking accounts for a larger fraction of EC than biomass burning. The interquartile ranges for $f_{liq.fossil}$ overlap with those for f_{coal} in winter and spring (Table S7). However, comparing the PDFs distribution for both cases give a more complete picture. As shown in Fig. 6, there is fair amount of overlap between the PDFs distributions of $f_{liq.fossil}$ and f_{ocal}. Though with some overlaps, in all seasons, the distribution of $f_{liq.fossil}$ are skewed to the left, while f_{coal} is skewed to the right, with considerably higher median $f_{liq.fossil}$ than median f_{coal}.

EC concentrations from biomass burning (EC_{bb}) increased by 9 times from summer (seasonal average of 0.2 µg m^{-3}) to winter (1.8 µg m^{-3}; Fig. 5b, Table S8). EC from coal combustion (EC_{coal}) has a 5-fold increase from about 0.3 µg m^{-3} in summer and autumn to 1.6 µg m^{-3} in winter. EC from liquid fossil fuel ($EC_{liq.fossil}$) varies less strongly than EC_{bb} and EC_{coal}, by 4-times from 0.7 µg m^{-3} in summer and 2.9 µg m^{-3} in winter. Liquid fossil fuel combustion (i.e., vehicle emissions) should be roughly constant throughout the year. The increased concentrations of $EC_{liq.fossil}$ in winter are most likely due to unfavorable meteorological conditions. An increase larger than a factor of 4 therefore suggests increasing emissions in winter. Compared to the 4-times increase in $EC_{liq.fossil}$ from summer to winter, EC_{coal} only increases by five times in winter, reflecting the moderate seasonal variation of $\delta^{13}C_{EC}$ (Fig. 4). Coal use for heating during wintertime has been decreasing since the year 2008/2009 (Ni et al., 2018), suggested by the more depleted wintertime $\delta^{13}C_{EC}$ in 2015/2016 than that in 2008/2009 (Fig. 4). The decreasing contribution from coal combustion to EC is consistent with the changes in energy consumption and the decreasing concentrations of coal combustion indicators (e.g., As and Pb) in Xi'an as found in pervious studies (Xu et al., 2016; Ni et al., 2018). The poor separation of fossil sources of EC into coal combustion and liquid fossil fuel combustion could be another reason, but it is difficult to quantify this effect due to our poor knowledge of $\delta^{13}C$ source endmembers.

3.4 Primary and secondary OC

Based on the EC tracer method, $OC_{o,nf}$ is representative of SOC_{nf}, or can be considered an upper limit of SOC_{nf} if cooking sources are significant. The fractions of primary OC (POC_{bb} and POC_{fossil}) and secondary OC ($OC_{o,nf}$, and SOC_{fossil}) in total OC are shown in Figure 7 and Table S4. On a yearly basis, the most important contributor to OC was $OC_{o,nf}$ (around 35%). For all samples, $OC_{o,nf}$ concentrations were higher than POC_{bb}, despite the wide range of total OC concentrations in different seasons. POC_{bb} contributed a relatively small fraction of OC (15–18%) in the warm period, which increased to 22% during winter when Xi'an was impacted significantly by biomass burning for heating and cooking. Enhanced biomass burning activities during wintertime in Xi'an have also been reported by measurements of markers for biomass burning such as levoglucosan and K$^+$ (T. Zhang et al., 2014; Shen et al., 2017). In winter, SOC_{fossil} was generally more abundant than POC_{fossil}, suggesting that secondary formation rather than primary emissions was a more important contributor to total OC_{fossil}. However, in the warm period, for fossil fuel derived OC (POC_{fossil} and SOC_{fossil}), primary emissions dominated over secondary formation (Figs. 7b, 7c). The SOC_{fossil}/OC_{fossil} ratios indicate that SOC_{fossil} contributes roughly 57% to OC_{fossil} in winter versus 37% in the warm period. However, the lower SOC_{fossil}/OC_{fossil} ratios in the warm period (especially in summer) than winter in this study is unexpected due to the favorable atmospheric conditions (e.g., higher temperature and stronger solar radiation). Much higher contribution of SOC_{fossil} to OC_{fossil} (an annual average of around 70%) was found in southern China (Y. L. Zhang et al., 2014). The importance of fossil derived SOC formation to fossil OC during wintertime was also found in other Chinese cities, including Beijing, Shanghai and Guangzhou (Zhang et al., 2015a).

As for OC from secondary origin (i.e., SOC_{fossil} and $OC_{o,nf}$), $65 \pm 4\%$ is derived from non-fossil sources throughout of the year, with decreased contribution during wintertime (~60%). Using multiple state-of-the-art analytical techniques (e.g., ^{14}C measurements and aerosol mass spectrometry), R. J. Huang et al. (2014) found higher non-fossil contribution to SOC (65–85%) in Xi'an and Guangzhou and lower non-fossil contribution to SOC (35–55%) in Beijing and Shanghai in winter 2013.

5   These findings underline the importance of the non-fossil contribution to SOC formation in Chinese megacities. The considerable differences in SOC composition in different cities might be due to the significant difference in SOC precursors from different emission sources and atmospheric processes.

3.5 Fossil WIOC vs. fossil EC

Figure 8a shows a scatter plot of $WIOC_{fossil}$ and EC_{fossil} concentrations. EC_{fossil} is emitted by the combustion of fossil fuels,

10   mainly coal combustion and vehicle emissions in Xi'an. $WIOC_{fossil}$ increases concurrently with EC_{fossil} suggests that primary emissions by fossil fuel combustion are an important source for $WIOC_{fossil}$ as well. However, a much higher slope of $WIOC_{fossil}$ against EC_{fossil} was found in winter when compared with warm periods, implying that $WIOC_{fossil}$ and EC_{fossil} originated from different fossil sources in winter and warm periods. In northern China, coal is used widely in winter for heating, which has higher primary OC/EC ratios than vehicle emissions.

15   The ratio of $WIOC_{fossil}$ to EC_{fossil} ($(WIOC/EC)_{fossil}$) can give real world constraints on primary OC/EC ratios of an integrated fossil source. In the warm period, individual $(WIOC/EC)_{fossil}$ measured in this study ranged from 0.62 to 1.1 (averaged 0.85 ± 0.14), falling into the range of typical primary OC/EC ratios for vehicle emissions in tunnel studies (Cheng et al., 2010; Dai et al., 2015; Cui et al., 2016), excluding sample Summer-L with the highest $(WIOC/EC)_{fossil}$ ratio of 1.4 (Fig. 8b). The higher $(WIOC/EC)_{fossil}$ for Summer-L is likely due to the less efficient removal of WIOC in cleaner periods in contrast to more

20   polluted periods during summertime. The more stagnant conditions in more polluted periods (Fig. 3) provide longer time for photochemical processes and SOC formation contributing formation of WSOC and result in decreased $(WIOC/EC)_{fossil}$ ratios as discussed in Sect. 3.2. The $(WIOC/EC)_{fossil}$ during wintertime averaged 1.6 ± 0.1, which is closer to the primary OC/EC ratios for coal combustion than that for vehicle emissions (Fig. 8b), suggesting coal combustion is an important fossil source in winter besides vehicle emissions. Higher $(WIOC/EC)_{fossil}$ ratios in winter than in the warm period is also found in Beijing

25   in northern China, with $(WIOC/EC)_{fossil}$ ratio of 1.6–2.4 in winter versus 0.7–1.2 in the warm period (Liu et al., 2018). However, no strong seasonal trends of $(WIOC/EC)_{fossil}$ ratios was found in southern Chinese cities, such as Shanghai (range: 1.2–1.6; Liu et al., 2018), Guangzhou (range: 0.7–1.4; Liu et al., 2018) and Hainan (around 1; Y. L. Zhang et al., 2014). Lower $(WIOC/EC)_{fossil}$ ratios were found in the Netherlands (0.6 ± 0.3; Dusek et al., 2017), Switzerland or Sweden (ranging roughly from 0.5 to 1; Szidat et al., 2004, 2009). Those higher values in China than in Europe could be attributed to the

30   combined effects of less efficient combustion of fuel in older vehicles in China and higher primary OC/EC ratios from coal combustion that is more common in China (especially in winter in northern China) than in Europe.

In warm period, most of individual $(WIOC/EC)_{fossil}$ falls in the range of primary OC/EC ratio for vehicle emissions, indicating that vehicle emission is the overwhelming fossil source with negligible contribution from coal combustion. However, EC source apportionment by combining $F^{14}C$ and $\delta^{13}C$ of EC in this study (Fig. 5) and previous studies in Xi'an (Wang et al., 2015; Ni et al., 2018) indicates that even in the warm period, coal combustion is also an important source of fine particles. Another inconsistency is that the considerable difference in $(WIOC/EC)_{fossil}$ between winter and warm period suggests strong seasonal variation of coal combustion, whereas only moderate seasonal changes of $\delta^{13}C_{EC}$ were observed. Possible causes of those contradictions will be explained in the following section.

3.6 Fossil OC: water-insoluble OC versus primary OC, water-soluble OC versus secondary OC

Fossil WIOC ($WIOC_{fossil}$) and WSOC ($WSOC_{fossil}$) have been used widely as proxies of the fossil POC (POC_{fossil}) and SOC (SOC_{fossil}), respectively (e.g., Liu et al., 2014; Y. L. Zhang et al., 2014), because primary OC from fossil sources are mainly WIOC. Figure 9 compares the mass concentrations of $WIOC_{fossil}$ with POC_{fossil}, as well as $WSOC_{fossil}$ with SOC_{fossil}. The wider uncertainty ranges of POC_{fossil} and SOC_{fossil} than ^{14}C-apportioned $WIOC_{fossil}$ and $WSOC_{fossil}$ are mainly propagated from wide range of primary OC/EC ratios for fossil emissions (Sect. 2.5).

The same trend is observed for $WIOC_{fossil}$ and POC_{fossil} throughout the year (Fig. 9a). In winter, the averaged $WIOC_{fossil}$ concentrations of 7.1 µg m^{-3} (range of 3.3–10.1 µg m^{-3}) matched the averaged POC_{fossil} concentrations of 6.0 µg m^{-3} (range of 2.7–9.2 µg m^{-3}). However, in the warm period, the $WIOC_{fossil}$ concentrations (1.8 µg m^{-3}, with a range of 0.8–5.4 µg m^{-3}) do not match the estimated POC_{fossil} (2.7 µg m^{-3}, with a range of 0.8–7.1 µg m^{-3}) equally well. $WIOC_{fossil}$ is still highly correlated with POC_{fossil} but deviates strongly from the 1:1 line of $WIOC_{fossil}$ against POC_{fossil}, with a linear regression having a slope of 1.31, and intercept of 0.32 and an R^2 of 0.92. The higher POC_{fossil} than $WIOC_{fossil}$ is well outside the measurement uncertainties, at least for most of samples representing high (H) and medium (M) TC concentrations (i.e., Spring-H, Spring-M, Summer-H, Autumn-H and Autumn-M). Previous studies have found that a part of WIOC can also be secondary origin from fossil sources in Egypt (Favez et al., 2008), France (Sciare et al., 2011) and Beijing, China (Zhang et al., 2018), but this would cause the opposite trend (higher $WIOC_{fossil}$ than POC_{fossil}). On the other hand, measurements of fresh emissions from fossil sources show that only a small fraction (~ 10%) of primary fossil OC is water-soluble (Dai et al., 2015; Yan et al., 2017). The differences between POC_{fossil} and $WIOC_{fossil}$ (25–55%) are much larger than that and therefore the small fraction of primary fossil WSOC can not explain the differences between POC_{fossil} and $WIOC_{fossil}$. The best explanation for the differences in summer and spring during polluted periods is the loss of fossil WIOC, indicated by decreased $(WIOC/EC)_{fossil}$ when pollution gets worse. This is probably due to more stagnant conditions in polluted periods, which allows for accumulation of pollutants and also more time for photochemical processing of WIOC and SOC formation, as discussed in Sect. 3.2. Evaporation of WIOC is not a likely explanation for this trend as temperatures do not differ strongly between clean and polluted periods and partitioning to the gas-phase should be stronger in clean conditions. However, this decreasing trend of $(WIOC/EC)_{fossil}$ with increasing TC is not found in autumn, where $WIOC_{fossil}$ is lower than estimated POC_{fossil} by a

roughly constant factor. In the fall wind speed is generally low and not very variable, and photochemical processing would be weaker than in the summer and spring.

Overall, the most likely explanation for the difference between $WIOC_{fossil}$ and POC_{fossil} is the overestimate of POC_{fossil} by the EC tracer method. POC_{fossil} is calculated by multiplying EC_{fossil} with primary OC/EC ratios for fossil sources (r_{fossil} in Eq. 11). Thus, an overestimate of POC_{fossil} result has two causes. First, r_{fossil} might be overestimated (as EC_{fossil} is well constrained by ^{14}C), which could result either from a too high estimated fraction of coal burning in the warm period, or through rapid evaporation of POC at warmer temperatures. In the warm period, semi-volatile OC from fossil emission sources partitions more readily to the gas-phase leading to lower primary OC/EC ratios compared to winter. This is supported by laboratory studies and ambient observations, which find that the primary OC/EC ratio for vehicle emissions is lower in warm period than in winter (Xie et al., 2017; X. H. H. Huang et al., 2014). Second, during longer residence time in the atmosphere POC might not be chemically stable and r_{fossil} decreases with aging time in the atmosphere. This is the only mechanism that can explain the decreasing $WIOC_{fossil}/EC_{fossil}$ ratios with higher pollutant concentrations and it is in line with findings from our earlier study that OC loss due to active photochemistry is more intense under high temperature and humidity in a warm period than in a cold winter (Ni et al., 2018).

As a consequence, a good match between $WSOC_{fossil}$ and SOC_{fossil} was observed in winter. As shown in Fig. 9d, the 3 data points fall close the 1:1 line of $WSOC_{fossil}$ against SOC_{fossil}. However, in the warm period, the data points fall below the 1:1 line of $WSOC_{fossil}$ against SOC_{fossil}, with a linear regression having a slope of 0.62, and intercept of 0.01 and an R^2 of 0.92. Higher $WSOC_{fossil}$ than SOC_{fossil} can be explained by either underestimated SOC_{fossil} or overestimated $WSOC_{fossil}$, or both. SOC_{fossil} is calculated by subtracting POC_{fossil} from OC_{fossil}. Thus, underestimated SOC_{fossil} in warm period can result directly from overestimated POC_{fossil} due to active OC loss.

The comparisons between $WIOC_{fossil}$ and POC_{fossil}, $WSOC_{fossil}$ and SOC_{fossil} suggest that it is feasible to use $WIOC_{fossil}$ and $WSOC_{fossil}$ as indicator of POC_{fossil} and SOC_{fossil}, respectively, with respect to trends and variations of POC_{fossil} and SOC_{fossil}. However, the absolute concentrations of $WIOC_{fossil}$ and $WSOC_{fossil}$ are not equal to those of respective estimated POC_{fossil} and SOC_{fossil}, especially in the warm period. If we consider photochemical loss as the primary reason of the differences between $WIOC_{fossil}$ and POC_{fossil}, $WSOC_{fossil}$ and SOC_{fossil}, then ^{14}C-based $WIOC_{fossil}$ and $WSOC_{fossil}$ are probably a better approximation for primary and secondary fossil OC, respectively, than POC_{fossil} and SOC_{fossil} estimated using the EC tracer method (Sect. 2.5, Eqs. 7–10).

4 Conclusions

This study presents the first source apportionment of various carbonaceous aerosol fractions, including EC, OC, WIOC and WSOC in Xi'an, China based on radiocarbon (^{14}C) measurement in four seasons for the year 2015/2016. [14]C analysis shows

that non-fossil sources are an important contributor to OC fractions throughout the year, accounting for $58 \pm 6\%$ WSOC, $53 \pm 4\%$ OC and $55 \pm 5\%$ WIOC, whereas fossil sources dominated EC, with non-fossil sources contributing $18 \pm 6\%$ EC on the yearly average. An increased contribution of non-fossil sources to all carbon fractions were observed in winter, because of enhanced non-fossil activities in winter, mainly biomass burning. Fossil sources of EC were further divided into liquid fossil fuel combustion (i.e., vehicle emissions) and coal combustion by combining radiocarbon and stable carbon signatures in a Bayesian Markov chain Monte Carlo (MCMC) approach. The MCMC results indicate that liquid fossil fuel combustion dominated EC over the whole year, contributing more than half of EC in the warm period and ~46% of EC in winter, despite the source changes in different seasons. The remaining fossil EC was contributed by coal combustion: in winter, coal combustion (~25%) and biomass burning (~28%) equally affected EC, whereas in the warm period, coal combustion contributed a larger fraction of EC than biomass burning did.

Concentrations of all carbon fractions were higher in winter than in the warm period. Non-fossil WSOC was responsible for ~35% of the increased OC mass in winter, followed by non-fossil WIOC (~24%), fossil WIOC (~ 22%; $WIOC_{fossil}$) and fossil WSOC (~ 19%; $WSOC_{fossil}$). Fossil EC and biomass burning EC on average accounted for 62 % and 38 % increased EC mass in winter. Fossil WIOC/EC ratios ($(WIOC/EC)_{fossil}$) in the warm period averaged 0.85 ± 0.14, well within the range of typical primary OC/EC ratios for vehicle emissions in tunnel studies (Cheng et al., 2010; Dai et al., 2015; Cui et al., 2016). Much higher $(WIOC/EC)_{fossil}$ values were found in winter, with an average of 1.6 ± 0.11, which is closer to the primary OC/EC ratios for coal combustion (2.38 ± 0.44; Sect. 2.5) than that for vehicle emissions, indicating additional contribution from coal burning in winter. Higher $(WIOC/EC)_{fossil}$ in winter than in the warm period is also found in Beijing in northern China (Liu et al., 2018). However, no strong seasonal trends of $(WIOC/EC)_{fossil}$ was found in southern China, such as Shanghai (Liu et al., 2018), Guangzhou (Liu et al., 2018) and Hainan (Y. L. Zhang et al., 2014), where there is no official heating season using coal.

The majority (60–76%) of the non-fossil OC was water-soluble in all seasons, probably resulting from the mostly water-soluble biomass-burning POC and SOC and biogenic SOC. The fossil OC in winter is less water-soluble than warm period, suggesting an enhanced SOC formation from fossil VOCs from vehicle emissions and/or coal burning in the warm period. In spring and summer, there is a clear increasing trend of $(WSOC/OC)_{fossil}$ and decreasing trend of $(WIOC/EC)_{fossil}$ in more polluted conditions. This suggests that the fossil WSOC formation as well as fossil WIOC removal increase under the stagnant conditions that characterize polluted periods and allow for accumulation of pollutants and also photochemical processing and secondary OC formation. $WIOC_{fossil}$ and $WSOC_{fossil}$ have been used widely as proxies of the primary and secondary fossil OC, respectively, since primary fossil sources tend to produce mainly WIOC. In winter, mass concentrations of $WIOC_{fossil}$ were comparable to POC_{fossil} and $WSOC_{fossil}$ to SOC_{fossil}, where POC_{fossil} and SOC_{fossil} are estimated using EC tracer method. However, the agreement was worse in the warm period, even though the respective concentrations were highly correlated. In other words, variations in $WIOC_{fossil}$ and $WSOC_{fossil}$ follow similar trends as

POC$_{fossil}$ and SOC$_{fossil}$, respectively. However, the absolute concentrations of WIOC$_{fossil}$ and WSOC$_{fossil}$ are not equal to those of estimated POC$_{fossil}$ and SOC$_{fossil}$, especially in the warm period. The higher mass of POC$_{fossil}$ than WIOC$_{fossil}$ in the warm period was probably due to overestimated POC$_{fossil}$ (thus underestimated SOC$_{fossil}$) resulted from overestimated primary fossil OC/EC ratios. In the warm period, at relatively high temperatures, semi-volatile OC from emission sources becomes

5 volatilized more quickly owing to higher temperatures, leading to lower primary OC/EC ratios than other seasons. This is in line with the laboratory and ambient observations that the primary OC/EC ratio for vehicle emissions is lower in the warm period than in winter (Xie et al., 2017; X. H. H. Huang et al., 2014), and the findings from our earlier study that in the warm period, that photochemical OC loss is active and affect final OC concentrations (Ni et al., 2018). We suggest that WIOC$_{fossil}$ and WSOC$_{fossil}$ are probably a better approximation for primary and secondary fossil OC, respectively, than POC$_{fossil}$ and

10 SOC$_{fossil}$ estimated using the EC tracer method.

Data availability

All data needed to evaluate the conclusions in this study are present in the paper and the Supplment. Additional data related to this paper are availabe upon request to the corresponding author.

Author contributions

15 UD, RJH, HN and JC designed the study. HN and HD conducted the ^{14}C measurements. HN, HD and UD interpreted the ^{14}C data. JG preformed the measurements of stable isotope [13]C. HN and UD interpreted the ^{13}C data. HN and UD prepared display items and HN wrote the mansucript. All authors commented on and discussed the manuscript.

Competing interests

The authors declare that they have no conflict of interest.

20 **Acknowledgments**

This work was supported by the National Key Research and Development Program of China (no. 2017YFC0212701), the National Natural Science Foundation of China (NSFC; no. 91644219 and 41877408), and a KNAW project (no. 530-5CDP30). The authors acknowledge the financial support from the Gratama Foundation. Special thanks are given to Dipayan Paul, Marc Bleeker and Henk Been for their help with the AMS measurements at CIO, and to Anita Aerts-Bijma and Dicky

25 van Zonneveld for her help with ^{14}C data correction at CIO.

References

Akagi, S. K., Yokelson, R. J., Wiedinmyer, C., Alvarado, M. J., Reid, J. S., Karl, T., Crounse, J. D., and Wennberg, P. O.: Emission factors for open and domestic biomass burning for use in atmospheric models, Atmos. Chem. Phys., 11, 4039-4072, https://doi.org/10.5194/acp-11-4039-2011, 2011.

5 Andersson, A., Deng, J., Du, K., Zheng, M., Yan, C., Sköld, M., and Gustafsson, Ö.: Regionally-varying combustion sources of the January 2013 severe haze events over eastern China, Environ. Sci. Technol., 49, 2038–2043, 2015.

Bernardoni, V., Calzolai, G., Chiari, M., Fedi, M., Lucarelli, F., Nava, S., Piazzalunga, A., Riccobono, F., Taccetti, F., Valli, G., and Vecchi, R.: Radiocarbon analysis on organic and elemental carbon in aerosol samples and source apportionment at an urban site in Northern Italy, J. Aerosol Sci., 56, 88–99, doi:10.1016/j.jaerosci.2012.06.001, 2013.

10 Cao, F., Zhang, Y., Ren, L., Liu, J., Li, J., Zhang, G., Liu, D., Sun, Y., Wang, Z., Shi, Z., and Fu, P.: New insights into the sources and formation of carbonaceous aerosols in China: potential applications of dual-carbon isotopes, Natl. Sci. Rev., 4, 804–806, 2017.

Cao, J. -J., Chow, J. C., Tao, J., Lee, S.C., Watson, J. G., Ho, K.F., Wang, G.H., Zhu, C.S., and Han, Y.M.: Stable carbon isotopes in aerosols from Chinese cities: influence of fossil fuels, Atmos. Environ., 45, 1359–1363, 2011.

15 Cao, J.-J., Shen, Z.-X., Chow, J. C., Watson, J. G., Lee, S.-C., Tie, X.-X., Ho, K.-F., Wang, G.-H., and Han, Y.-M.: Winter and summer $PM_{2.5}$ chemical compositions in fourteen Chinese cities, J. Air Waste Manage., 62, 1214-1226, https://doi.org/10.1080/10962247.2012.701193, 2012.

Cao, J.-J., Zhu, C.-S., Tie, X.-X., Geng, F.-H., Xu, H.-M., Ho, S. S. H., Wang, G.-H., Han, Y.-M., and Ho, K.-F.: Characteristics and sources of carbonaceous aerosols from Shanghai, China, Atmos. Chem. Phys., 13, 803-817, 20 https://doi.org/10.5194/acp-13-803-2013, 2013.

Cavalli, F., Viana, M., Yttri, K. E., Genberg, J., and Putaud, J.-P.: Toward a standardised thermal-optical protocol for measuring atmospheric organic and elemental carbon: the EUSAAR protocol, Atmos. Meas. Tech., 3, 79-89, https://doi.org/10.5194/amt-3-79-2010, 2010.

Cheng, C., Wang, G., Zhou, B., Meng, J., Li, J., Cao, J., and Xiao, S.: Comparison of dicarboxylic acids and related 25 compounds in aerosol samples collected in Xi'an, China during haze and clean periods, Atmos. Environ., 81, 443-449, 2013.

Cheng, Y., Lee, S. C., Ho, K. F., Chow, J. C., Watson, J. G., Louie, P. K. K., Cao, J. J., and Hai, X.: Chemically-speciated on-road $PM_{2.5}$ motor vehicle emission factors in Hong Kong, Sci. Total Environ., 408, 1621-1627, http://dx.doi.org/10.1016/j.scitotenv.2009.11.061, 2010.

Cui, M., Chen, Y., Tian, C., Zhang, F., Yan, C., and Zheng, M.: Chemical composition of $PM_{2.5}$ from two tunnels with 30 different vehicular fleet characteristics, Sci. Total Environ., 550, 123-132, http://dx.doi.org/10.1016/j.scitotenv.2016.01.077, 2016.

Dai, S., Bi, X., Chan, L. Y., He, J., Wang, B., Wang, X., Peng, P., Sheng, G., and Fu, J.: Chemical and stable carbon isotopic composition of $PM_{2.5}$ from on-road vehicle emissions in the PRD region and implications for vehicle emission control policy, Atmos. Chem. Phys., 15, 3097-3108, https://doi.org/10.5194/acp-15-3097-2015, 2015.

35 Dusek, U., Ten Brink, H., Meijer, H., Kos, G., Mrozek, D., Röckmann, T., Holzinger, R., and Weijers, E.: The contribution of fossil sources to the organic aerosol in the Netherlands, Atmos. Environ., 74, 169-176, 2013.

Dusek, U., Monaco, M., Prokopiou, M., Gongriep, F., Hitzenberger, R., Meijer, H. A. J., and Röckmann, T.: Evaluation of a two-step thermal method for separating organic and elemental carbon for radiocarbon analysis, Atmos. Meas. Tech., 7, 1943-1955, https://doi.org/10.5194/amt-7-1943-2014, 2014.

40 Dusek, U., Hitzenberger, R., Kasper-Giebl, A., Kistler, M., Meijer, H. A. J., Szidat, S., Wacker, L., Holzinger, R., and Röckmann, T.: Sources and formation mechanisms of carbonaceous aerosol at a regional background site in the Netherlands:

insights from a year-long radiocarbon study, Atmos. Chem. Phys., 17, 3233-3251, https://doi.org/10.5194/acp-17-3233-2017, 2017.

Elser, M., Huang, R.-J., Wolf, R., Slowik, J. G., Wang, Q., Canonaco, F., Li, G., Bozzetti, C., Daellenbach, K. R., Huang, Y., Zhang, R., Li, Z., Cao, J., Baltensperger, U., El-Haddad, I., and Prévôt, A. S. H.: New insights into $PM_{2.5}$ chemical composition and sources in two major cities in China during extreme haze events using aerosol mass spectrometry, Atmos. Chem. Phys., 16, 3207-3225, https://doi.org/10.5194/acp-16-3207-2016, 2016.

Fang, W., Du, K., Andersson, A., Xing, Z., Cho, C., Kim, S. W., Deng, J., and Gustafsson, Ö.: Dual-isotope constraints on seasonally-resolved source fingerprinting of Black Carbon aerosols in sites of the four emission hotspot regions of China, J. Geophys. Res.-Atmos., 123, 11735-11747, https://doi.org/10.1029/2018JD028607, 2018.

Favez, O., Sciare, J., Cachier, H., Alfaro, S. C., and Abdelwahab, M. M.: Significant formation of water-insoluble secondary organic aerosols in semi-arid urban environment, Geophys. Res. Lett., 35, L15801, https://doi.org/10.1029/2008GL034446, 2008.

Gelencsér, A., May, B., Simpson, D., Sánchez‐Ochoa, A., Kasper‐Giebl, A., Puxbaum, H., Caseiro, A., Pio, C., and Legrand, M.: Source apportionment of PM2.5 organic aerosol over Europe: Primary/secondary, natural/anthropogenic, and fossil/biogenic origin, J. Geophys. Res., 112, D23S04, doi:10.1029/2006JD008094, 2007.

Guo, S., Hu, M., Guo, Q., Zhang, X., Zheng, M., Zheng, J., Chang, C. C., Schauer, J. J., and Zhang, R.: Primary sources and secondary formation of organic aerosols in Beijing, China, Environ. Sci. Technol., 46, 9846–9853, 2012.

Gustafsson, Ö., Kruså, M., Zencak, Z., Sheesley, R. J., Granat, L., Engström, E., Praveen, P., Rao, P., Leck, C., and Rodhe, H.: Brown clouds over South Asia: biomass or fossil fuel combustion?, Science, 323, 495-498, 2009.

Hallquist, M., Wenger, J. C., Baltensperger, U., Rudich, Y., Simpson, D., Claeys, M., Dommen, J., Donahue, N. M., George, C., Goldstein, A. H., Hamilton, J. F., Herrmann, H., Hoffmann, T., Iinuma, Y., Jang, M., Jenkin, M. E., Jimenez, J. L., Kiendler-Scharr, A., Maenhaut, W., McFiggans, G., Mentel, Th. F., Monod, A., Prévôt, A. S. H., Seinfeld, J. H., Surratt, J. D., Szmigielski, R., and Wildt, J.: The formation, properties and impact of secondary organic aerosol: current and emerging issues, Atmos. Chem. Phys., 9, 5155-5236, https://doi.org/10.5194/acp-9-5155-2009, 2009.

Heal, M. R.: The application of carbon-14 analyses to the source apportionment of atmospheric carbonaceous particulate matter: a review, Anal. Bioanal. Chem., 406, 81-98, 2014.

Hua, Q. and Barbetti, M.: Review of tropospheric bomb ^{14}C data for carbon cycle modeling and age calibration purposes, Radiocarbon, 46, 1273-1298, 2004.

Huang, R. J., Zhang, Y., Bozzeti, C., Ho, K. F., Cao, J. J., Han, Y., Daellenbach, K. R., Slowik, J.G., Platt, S. M., Canonaco, F., Zotter, P., Wolf, R., Pieber, S. M., Bruns, E. A., Crippa, M., Ciarelli, G., Piazzalunga, A., Schwikowski, M., Abbaszade, G., SchnelleKreis, J., Zimmermann, R., An, Z., Szidat, S., Baltensperger, U., El Haddad, I., and Prévôt, A. S. H.: High secondary aerosol contribution to particulate pollution during haze events in China, Nature, 514, 218–222, doi:10.1038/nature13774, 2014.

Huang, X., Li, M., Li, J., and Song, Y.: A high-resolution emission inventory of crop burning in fields in China based on MODIS Thermal Anomalies/Fire products, Atmos. Environ., 50, 9-15, 2012.

Huang, X. H. H., Bian, Q. J., Louie, P. K. K., and Yu, J. Z.: Contributions of vehicular carbonaceous aerosols to $PM_{2.5}$ in a roadside environment in Hong Kong, Atmos. Chem. Phys., 14, 9279-9293, https://doi.org/10.5194/acp-14-9279-2014, 2014.

Irei, S., Rudolph, J., Huang, L., Auld, J., and Hastie, D.: Stable carbon isotope ratio of secondary particulate organic matter formed by photooxidation of toluene in indoor smog chamber, Atmos. Environ., 45, 856–862, 2011.

Jacobson, M. C., Hansson, H. C., Noone, K. J., and Charlson, R. J.: Organic atmospheric aerosols: review and state of the science, Rev. Geophys., 38, 267–294, 2000.

Kanakidou, M., Seinfeld, J. H., Pandis, S. N., Barnes, I., Dentener, F. J., Facchini, M. C., Van Dingenen, R., Ervens, B., Nenes, A., Nielsen, C. J., Swietlicki, E., Putaud, J. P., Balkanski, Y., Fuzzi, S., Horth, J., Moortgat, G. K., Winterhalter, R., Myhre, C. E. L., Tsigaridis, K., Vignati, E., Stephanou, E. G., and Wilson, J.: Organic aerosol and global climate modelling: a review, Atmos. Chem. Phys., 5, 1053-1123, https://doi.org/10.5194/acp-5-1053-2005, 2005.

5   Kondo, Y., Miyazaki, Y., Takegawa, N., Miyakawa, T., Weber, R. J., Jimenez, J. L., Zhang, Q., and Worsnop, D. R.: Oxygenated and water-soluble organic aerosols in Tokyo, J. Geophys. Res.-Atmos., 112, D01203, doi:10.1029/2006JD007056, 2007.

Levin, I., B. Kromer, and Hammer, S.: Atmospheric $\Delta^{14}CO_2$ trend in Western European background air from 2000 to 2012, Tellus B, 65, 20092, doi: 10.3402/tellusb.v65i0.20092, 2013.

10 Levin, I., Hammer, S., Kromer, B., and Meinhardt, F.: Radiocarbon observations in atmospheric CO_2: determining fossil fuel CO_2 over Europe using Jungfraujoch observations as background, Sci. Total Environ., 391, 211-216, 2008.

Levin, I., Naegler, T., Kromer, B., Diehl, M., Francey, R. J., Gomez-Pelaez, A., Steele, P., Wagenbach, D., Weller, R., and Worthy, D.: Observations and modelling of the global distribution and long-term trend of atmospheric $^{14}CO_2$, Tellus B, 62, 26–46, 2010.

15 Lewis, C. W., Klouda, G. A., and Ellenson, W. D.: Radiocarbon measurement of the biogenic contribution to summertime PM-2.5 ambient aerosol in Nashville, TN, Atmos. Environ., 38, 6053–6061, 2004.

Li, C., Bosch, C., Kang, S., Andersson, A., Chen, P., Zhang, Q., Cong, Z., Chen, B., Qin, D., and Gustafsson, Ö.: Sources of black carbon to the Himalayan–Tibetan Plateau glaciers, Nat. Commun., 7, 12574, doi: 10.1038/ncomms12574, 2016.

Liu, D., Li, J., Zhang, Y., Xu, Y., Liu, X., Ding, P., Shen, C., Chen, Y., Tian, C., and Zhang, G.: The use of levoglucosan
20 and radiocarbon for source apportionment of $PM_{2.5}$ carbonaceous aerosols at a background site in East China, Environ. Sci. Technol., 47, 10454–10461, 2013.

Liu, D., Li, J., Cheng, Z., Zhong, G., Zhu, S., Ding, P., Shen, C., Tian, C., Chen, Y., Zhi, G., and Zhang, G.: Sources of non-fossil-fuel emissions in carbonaceous aerosols during early winter in Chinese cities, Atmos. Chem. Phys., 17, 11491-11502, https://doi.org/10.5194/acp-17-11491-2017, 2017.

25 Liu, D., Vonwiller, M., Li, J., Liu, J., Szidat, S., Zhang, Y., Tian, C., Chen, Y., Cheng, Z., Zhong, G., Fu, P., and Zhang, G.: Fossil and non-fossil sources of organic and elemental carbon aerosols in Beijing, Shanghai and Guangzhou: seasonal variation of carbon source, Atmos. Chem. Phys. Discuss., https://doi.org/10.5194/acp-2018-295, 2018.

Liu, J., Li, J., Zhang, Y., Liu, D., Ding, P., Shen, C., Shen, K., He, Q., Ding, X., Wang, X., Chen, D., and Zhang, G.: Source apportionment using radiocarbon and organic tracers for $PM_{2.5}$ carbonaceous aerosols in Guangzhou, South China:
30 contrasting local-and regional-scale aaze events, Environ. Sci. Technol., 48, 12002–12011, 2014.

Liu, J., Li, J., Liu, D., Ding, P., Shen, C., Mo, Y., Wang, X., Luo, C., Cheng, Z., Szidat, S., Zhang, Y., Chen, Y., and Zhang, G.: Source apportionment and dynamic changes of carbonaceous aerosols during the haze bloom-decay process in China based on radiocarbon and organic molecular tracers, Atmos. Chem. Phys., 16, 2985-2996, https://doi.org/10.5194/acp-16-2985-2016, 2016a.

35 Liu, J., Li, J., Vonwiller, M., Liu, D., Cheng, H., Shen, K., Salazar, G., Agrios, K., Zhang, Y., He, Q., Ding, X., Zhong, G., Wang, X., Szidat, S., and Zhang, G.: The importance of non-fossil sources in carbonaceous aerosols in a megacity of central China during the 2013 winter haze episode: a source apportionment constrained by radiocarbon and organic tracers, Atmos. Environ., 144, 60–68, 2016b.

Mayol-Bracero, O. L., Guyon, P., Graham, B., Roberts, G., Andreae, M. O., Decesari, S., Facchini, M. C., Fuzzi, S.,
40 and Artaxo, P.: Water-soluble organic compounds in biomass burning aerosols over Amazonia, 2, apportionment of the chemical composition and importance of the polyacidic fraction, J. Geophys. Res.-Atmos., 107(D20), 8091, doi:10.1029/2001JD000522, 2002.

Miyazaki, Y., Kondo, Y., Takegawa, N., Komazaki, Y., Fukuda, M., Kawamura, K., Mochida, M., Okuzawa, K., and Weber, R. J.: Time-resolved measurements of water-soluble organic carbon in Tokyo, J. Geophys. Res.-Atmos., 111, D23206, doi:10.1029/2006JD007125, 2006

5   Mohn, J., Szidat, S., Fellner, J., Rechberger, H., Quartier, R., Buchmann, B., and Emmenegger, L.: Determination of biogenic and fossil CO_2 emitted by waste incineration based on $^{14}CO_2$ and mass balances, Bioresource Technol., 99, 6471–6479, 2008.

Mook, W. G. and van der Plicht, J.: Reporting ^{14}C activities and concentrations, Radiocarbon, 41, 227–239, 1999.

Ni, H., Tian, J., Wang, X., Wang, Q., Han, Y., Cao, J., Long, X., Chen, L. W. A., Chow, J. C., Watson, J. G., Huang, R.-J., and Dusek, U.: $PM_{2.5}$ emissions and source profiles from open burning of crop residues, Atmos. Environ., 169, 229-237, 10   https://doi.org/10.1016/j.atmosenv.2017.08.063, 2017.

Ni, H., Huang, R.-J., Cao, J., Liu, W., Zhang, T., Wang, M., Meijer, H. A. J., and Dusek, U.: Source apportionment of carbonaceous aerosols in Xi'an, China: insights from a full year of measurements of radiocarbon and the stable isotope ^{13}C, Atmos. Chem. Phys., 18, 16363-16383, https://doi.org/10.5194/acp-18-16363-2018, 2018.

Nozière, B., Kalberer, M., Claeys, M., Allan, J., D'Anna, B., Decesari, S., Finessi, E., Glasius, M., Grgić, I., Hamilton, J. F., 15   Hoffmann, T., Iinuma, Y., Jaoui, M., Kahnt, A., Kampf, C. J., Kourtchev, I., Maenhaut, W., Marsden, N., Saarikoski, S., Schnelle-Kreis, J., Surratt, J. D., Szidat, S., Szmigielski, R., and Wisthaler, A.: The molecular identification of organic compounds in the atmosphere: state of the art and challenges, Chem. Rev., 115, 3919-3983, 10.1021/cr5003485, 2015.

Palstra, S. W. and Meijer, H. A.: Biogenic carbon fraction of biogas and natural gas fuel mixtures determined with ^{14}C, Radiocarbon, 56, 7-28, 2014.

20   Parnell, A. C., Inger, R., Bearhop, S., and Jackson, A. L.: Source partitioning using stable isotopes: coping with too much variation, PloS ONE, 5, e9672, 2010.

Parnell, A. C., Phillips, D. L., Bearhop, S., Semmens, B. X., Ward, E. J., Moore, J. W., Jackson, A. L., Grey, J., Kelly, D. J., and Inger, R.: Bayesian stable isotope mixing models, Environmetrics, 24, 387-399, 2013.

Pavuluri, C. M. and Kawamura, K.: Enrichment of ^{13}C in diacids and related compounds during photochemical processing of 25   aqueous aerosols: new proxy for organic aerosols aging, Sci. Rep., 6, 36467, 2016.

Pöschl, U.: Atmospheric aerosols: composition, transformation, climate and health effects, Angew. Chem. Int. Ed. Engl., 44, 7520-7540, 2005.

Reimer, P. J., Brown, T. A., and Reimer, R. W.: Discussion: reporting and calibration of post-bomb ^{14}C data, Radiocarbon, 46, 1299–1304, 2004.

30   Ruff, M., Wacker, L., Gäggeler, H., Suter, M., Synal, H.-A., and Szidat, S.: A gas ion source for radiocarbon measurements at 200 kV, Radiocarbon, 49, 307-314, 2007.

Salazar, G., Zhang, Y. L., Agrios, K., and Szidat, S.: Development of a method for fast and automatic radiocarbon measurement of aerosol samples by online coupling of an elemental analyzer with a MICADAS AMS, Nucl. Instrum. Meth. B, 361, 163-167, https://doi.org/10.1016/j.nimb.2015.03.051, 2015.

35   Sannigrahi, P., Sullivan, A. P., Weber, R. J., and Ingall, E. D.: Characterization of water-soluble organic carbon in urban atmospheric aerosols using solid-state ^{13}C NMR spectroscopy, Environ. Sci. Technol., 40, 666-672, 2006.

Sciare, J., d'Argouges, O., Sarda-Estève, R., Gaimoz, C., Dolgorouky, C., Bonnaire, N., Favez, O., Bonsang, B., and Gros, V.: Large contribution of water-insoluble secondary organic aerosols in the region of Paris (France) during wintertime, J. Geophys. Res.-Atmos., 116, D22203, doi:10.1029/2011JD015756, 2011.

40   Sheesley, R. J., Kirillova, E., Andersson, A., Kruså, M., Praveen, P., Budhavant, K., Safai, P. D., Rao, P., and Gustafsson, Ö.: Year-round radiocarbon-based source apportionment of carbonaceous aerosols at two background sites in South Asia, J. Geophys. Res.-Atmos., 117, 2012.

Shen, Z., Lei, Y., Zhang, L., Zhang, Q., Zeng, Y., Tao, J., Zhu, C., Cao, J., Xu, H., and Liu, S.: Methanol extracted brown carbon in PM$_{2.5}$ over Xi'an, China: seasonal variation of optical properties and sources identification, Aerosol Sci. Eng., 1, 57-65, 1-9, 10.1007/s41810-017-0007-z, 2017.

Streets, D., Yarber, K., Woo, J. H., and Carmichael, G.: Biomass burning in Asia: annual and seasonal estimates and atmospheric emissions, Global Biogeochem. Cy., 17, 1099, https://doi.org/10.1029/2003GB002040, 2003.

Stuiver, M. and Polach, H. A.: Discussion: Reporting of ^{14}C data, Radiocarbon, 19, 355–363, 1977.

Sun, J., Shen, Z., Cao, J., Zhang, L., Wu, T., Zhang, Q., Yin, X., Lei, Y., Huang, Y., Huang, R., Liu, S., Han, Y., Xu, H., Zheng, C., and Liu, P.: Particulate matters emitted from maize straw burning for winter heating in rural areas in Guanzhong Plain, China: current emission and future reduction, Atmos. Res., 184, 66–76, 2017.

Synal, H.-A., Stocker, M., and Suter, M.: MICADAS: A new compact radiocarbon AMS system, Nucl. Instrum. Meth. B, 259, 7-13, https://doi.org/10.1016/j.nimb.2007.01.138, 2007.

Szidat, S., Jenk, T. M., Gäggeler, H. W., Synal, H. A., Fisseha, R., Baltensperger, U., Kalberer, M., Samburova, V., Reimann, S., Kasper-Giebl, A., and Hajdas, I.: Radiocarbon (^{14}C)-deduced biogenic and anthropogenic contributions to organic carbon (OC) of urban aerosols from Zürich, Switzerland, Atmos. Environ., 38, 4035-4044, https://doi.org/10.1016/j.atmosenv.2004.03.066, 2004.

Szidat, S., Ruff, M., Perron, N., Wacker, L., Synal, H.-A., Hallquist, M., Shannigrahi, A. S., Yttri, K. E., Dye, C., and Simpson, D.: Fossil and non-fossil sources of organic carbon (OC) and elemental carbon (EC) in Göteborg, Sweden, Atmos. Chem. Phys., 9, 1521-1535, https://doi.org/10.5194/acp-9-1521-2009, 2009.

Szidat, S., Bench, G., Bernardoni, V., Calzolai, G., Czimczik, C.I., Derendorp, L., Dusek, U., Elder, K., Fedi, M.E., Genberg, J., Gustafsson, Ö., Kirillova, E., Kondo, M., McNichol, A. P., Perron, N., Santos, G. M., Stenström. K., Swietlicki, E., Uchida, M., Vecchi, R., Wacher, L., Zhang, Y., and Prévôt, A. S. H.: Intercomparison of ^{14}C analysis of carbonaceous aerosols: exercise 2009. Radiocarbon, 55, 1496-1509, 2013.

Tao, J., Zhang, L., Cao, J., and Zhang, R.: A review of current knowledge concerning PM$_{2.5}$ chemical composition, aerosol optical properties and their relationships across China, Atmos. Chem. Phys., 17, 9485-9518, https://doi.org/10.5194/acp-17-9485-2017, 2017.

Vlachou, A., Daellenbach, K. R., Bozzetti, C., Chazeau, B., Salazar, G. A., Szidat, S., Jaffrezo, J.-L., Hueglin, C., Baltensperger, U., Haddad, I. E., and Prévôt, A. S. H.: Advanced source apportionment of carbonaceous aerosols by coupling offline AMS and radiocarbon size-segregated measurements over a nearly 2-year period, Atmos. Chem. Phys., 18, 6187–6206, https://doi.org/10.5194/acp-18-6187-2018, 2018.

Wacker, L., Christl, M., and Synal, H. A.: Bats: A new tool for AMS data reduction, Nucl. Instrum. Meth. B, 268, 976-979, https://doi.org/10.1016/j.nimb.2009.10.078, 2010.

Wang, P., Cao, J.J., Shen, Z. X., Han, Y. M., Lee, S. C., Huang, Y., Zhu, C. S., Wang, Q. Y., Xu, H. M., and Huang, R. J.: Spatial and seasonal variations of PM$_{2.5}$ mass and species during 2010 in Xi'an, China, Sci. Total Environ., 508, 477-487, 2015.

Weber, R. J., Sullivan, A. P., Peltier, R. E., Russell, A., Yan, B., Zheng, M., de Gouw, J., Warneke, C., Brock, C., Holloway, J. S., Atlas, E. L., and Edgerton, E.: A study of secondary organic aerosol formation in the anthropogenic-influenced southeastern United States, J. Geophys. Res.-Atmos., 112, D13302, doi:10.1029/2007JD008408, 2007.

Winiger, P., Andersson, A., Yttri, K. E., Tunved, P., and Gustafsson, Ö.: Isotope-based source apportionment of EC aerosol particles during winter high-pollution events at the Zeppelin Observatory, Svalbard, Environ. Sci. Technol., 49, 11959–11966, 10.1021/acs.est.5b02644, 2015.

Winiger, P., Andersson, A., Eckhardt, S., Stohl, A., and Gustafsson, Ö.: The sources of atmospheric black carbon at a European gateway to the Arctic, Nat. Commun., 7, 2016.

Wozniak, A. S., Bauer, J. E., and Dickhut, R. M.: Characteristics of water-soluble organic carbon associated with aerosol particles in the eastern United States, Atmos. Environ., 46, 181-188, 2012.

Xie, M., Hays, M., and Holder, A.: Light-absorbing organic carbon from prescribed and laboratory biomass burning and gasoline vehicle emissions, Sci. Rep., 7, 7318, 2017.

5 Xu, H., Cao, J., Chow, J. C., Huang, R.-J., Shen, Z., Chen, L. A., Ho, K. F., and Watson, J. G.: Inter-annual variability of wintertime $PM_{2.5}$ chemical composition in Xi'an, China: evidences of changing source emissions, Sci. Total Environ., 545, 546–555, 2016.

Yan, C., Zheng, M., Bosch, C., Andersson, A., Desyaterik, Y., Sullivan, A. P., Collett, J. L., Zhao, B., Wang, S., He, K. and Gustafsson, Ö.: Important fossil source contribution to brown carbon in Beijing during winter, Sci. Rep., 7, 2017.

10 Zenker, K., Vonwiller, M., Szidat, S., Calzolai, G., Giannoni, M., Bernardoni, V., Jedynska, A. D., Henzing, B., Meijer, H. A., and Dusek, U.: Evaluation and inter-comparison of oxygen-based OC-EC separation methods for radiocarbon analysis of ambient aerosol particle samples, Atmosphere, 8, 226, 2017.

Zhang, T., Cao, J.-J., Chow, J. C., Shen, Z.-X., Ho, K.-F., Ho, S. S. H., Liu, S.-X., Han, Y.-M., Watson, J. G., Wang, G.-H., and Huang, R.-J.: Characterization and seasonal variations of levoglucosan in fine particulate matter in Xi'an, China, J. Air 15 Waste Manage., 64, 1317–1327, 10.1080/10962247.2014.944959, 2014.

Zhang, Y. L., Perron, N., Ciobanu, V. G., Zotter, P., Minguillón, M. C., Wacker, L., Prévôt, A. S. H., Baltensperger, U., and Szidat, S.: On the isolation of OC and EC and the optimal strategy of radiocarbon-based source apportionment of carbonaceous aerosols, Atmos. Chem. Phys., 12, 10841-10856, https://doi.org/10.5194/acp-12-10841-2012, 2012.

Zhang, Y. L., Zotter, P., Perron, N., Prévôt, A. S. H., Wacker, L., and Szidat, S.: Fossil and non-fossil sources of different 20 carbonaceous fractions in fine and coarse particles by radiocarbon measurement, Radiocarbon, 55, 1510-1520, 2013.

Zhang, Y. L., Li, J., Zhang, G., Zotter, P., Huang, R.-J., Tang, J.-H., Wacker, L., Prévôt, A. S. H., and Szidat, S.: Radiocarbon-based source apportionment of carbonaceous aerosols at a regional background site on Hainan Island, South China, Environ. Sci. Technol., 48, 2651–2659, 10.1021/es4050852, 2014.

Zhang, Y. L., Huang, R. J., El Haddad, I., Ho, K. F., Cao, J. J., Han, Y., Zotter, P., Bozzetti, C., Daellenbach, K. R., 25 Canonaco, F., Slowik, J. G., Salazar, G., Schwikowski, M., Schnelle-Kreis, J., Abbaszade, G., Zimmermann, R., Baltensperger, U., Prévôt, A. S. H., and Szidat, S.: Fossil vs. non-fossil sources of fine carbonaceous aerosols in four Chinese cities during the extreme winter haze episode of 2013, Atmos. Chem. Phys., 15, 1299-1312, https://doi.org/10.5194/acp-15-1299-2015, 2015a.

Zhang, Y. L., Schnelle-Kreis, J., Abbaszade, G., Zimmermann, R., Zotter, P., Shen, R. R., Schäefer, K., Shao, L., Prévôt, A , 30 and Szidat, S.: Source apportionment of elemental carbon in Beijing, China: insights from radiocarbon and organic marker measurements, Environ. Sci. Technol., 49, 8408–8415, 2015b.

Zhang, Y. L., Ren, H., Sun, Y., Cao, F., Chang, Y., Liu, S., Lee, X., Agrios, K., Kawamura, K., Liu, D., Ren, L., Du, W., Wang, Z., Prévôt, A. S. H., Szidat, S., and Fu, P.: High contribution of nonfossil sources to submicrometer organic aerosols in Beijing, China, Environ. Sci. Technol., 51, 7842–7852, 2017.

35 Zhang, Y.-L., El-Haddad, I., Huang, R.-J., Ho, K.-F., Cao, J.-J., Han, Y., Zotter, P., Bozzetti, C., Daellenbach, K. R., Slowik, J. G., Salazar, G., Prévôt, A. S. H., and Szidat, S.: Large contribution of fossil fuel derived secondary organic carbon to water soluble organic aerosols in winter haze in China, Atmos. Chem. Phys., 18, 4005-4017, https://doi.org/10.5194/acp-18-4005-2018, 2018.

Zhao, Z., Cao, J., Zhang, T., Shen, Z., Ni, H., Tian, J., Wang, Q., Liu, S., Zhou, J., Gu, J., and Shen, G.: Stable carbon 40 isotopes and levoglucosan for $PM_{2.5}$ elemental carbon source apportionments in the largest city of Northwest China, Atmos. Environ., 185, 253-261, https://doi.org/10.1016/j.atmosenv.2018.05.008, 2018.

Zhou, Y., Xing, X., Lang, J., Chen, D., Cheng, S., Wei, L., Wei, X., and Liu, C.: A comprehensive biomass burning emission inventory with high spatial and temporal resolution in China, Atmos. Chem. Phys., 17, 2839-2864, https://doi.org/10.5194/acp-17-2839-2017, 2017.

Zhu, C. S., Cao, J. J., Tsai, C. J., Zhang, Z. S., and Tao, J.: Biomass burning tracers in rural and urban ultrafine particles in Xi'an, China, Atmos. Pollut. Res., 8, 614–618, http://dx.doi.org/10.1016/j.apr.2016.12.011, 2017.
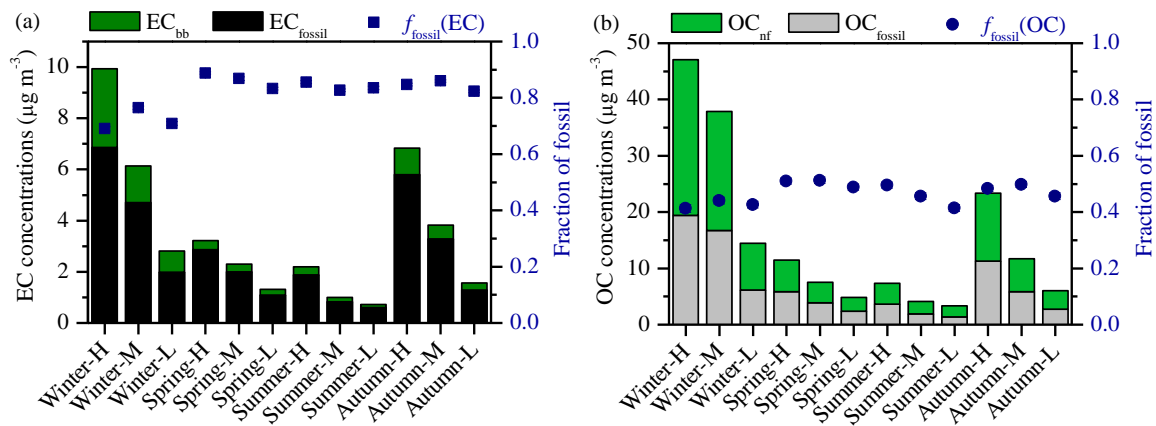
Figure 1. (a) Mass concentrations of EC from fossil and non-fossil sources (EC$_{fossil}$ and EC$_{bb}$, respectively), and fraction of fossil in EC (f_{fossil}(EC)). **(b)** Mass concentrations of OC from fossil and non-fossil sources (OC$_{fossil}$ and OC$_{nf}$, respectively), and fraction of fossil in OC (f_{fossil}(OC)).
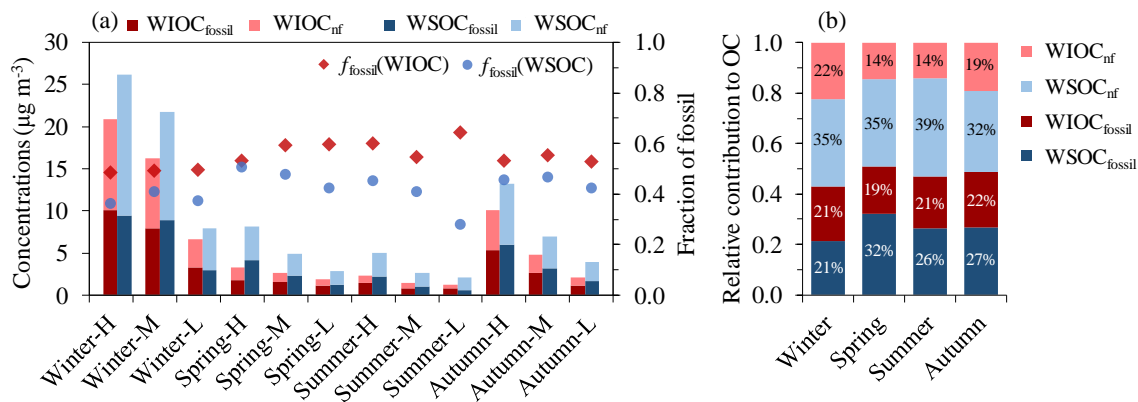
Figure 2. (a) Mass concentrations of WIOC and WSOC from fossil and non-fossil sources (WIOC$_{fossil}$, WIOC$_{nf}$, WSOC$_{fossil}$ and WSOC$_{nf}$) as well as fraction of fossil in WIOC and WSOC (f_{fossil}(WIOC) and f_{fossil}(WSOC), respectively). **(b)** Averaged relative contribution to OC (%) from WIOC$_{nf}$, WSOC$_{nf}$, WIOC$_{fossil}$, and WSOC$_{fossil}$ in each season.

Figure 3. (a) Wind speed for each composite sample. Each composite sample consists of 2–4 24h filter samples, and each filter sample is shown as individual datapoint. The wind speed is recorded by the Meteorological Institute of Shaanxi Province, Xi'an, China. **(b)** The fraction of fossil WSOC in fossil OC ((WSOC/OC)$_{fossil}$, dark blue circle), the fossil WIOC to fossil EC ratio ((WIOC/EC)$_{fossil}$, black square) over all the selected samples throughout the year.

Figure 4. The ^{14}C-based fraction fossil versus δ^{13}C for EC in Xi'an, China in different seasons in 2015/2016 (this study, circle symbols), compared with those in winter 2008/2009 from Ni et al. (2018) (square symbols). The size of the symbols for the year 2015/2016 (this study) represents the pollution conditions (high, medium and low) for each sample. The expected ^{14}C and δ^{13}C endmember ranges for emissions from C3 plant burning, liquid fossil fuel burning and coal burning are shown as green, black and brown bars, respectively. The δ^{13}C signatures are indicated as mean ± SD (Sect. 2.6). The δ^{13}C signatures of corn stalk (i.e., C4 plant) burning is -16.4 ± 1.4 ‰ is also indicated.
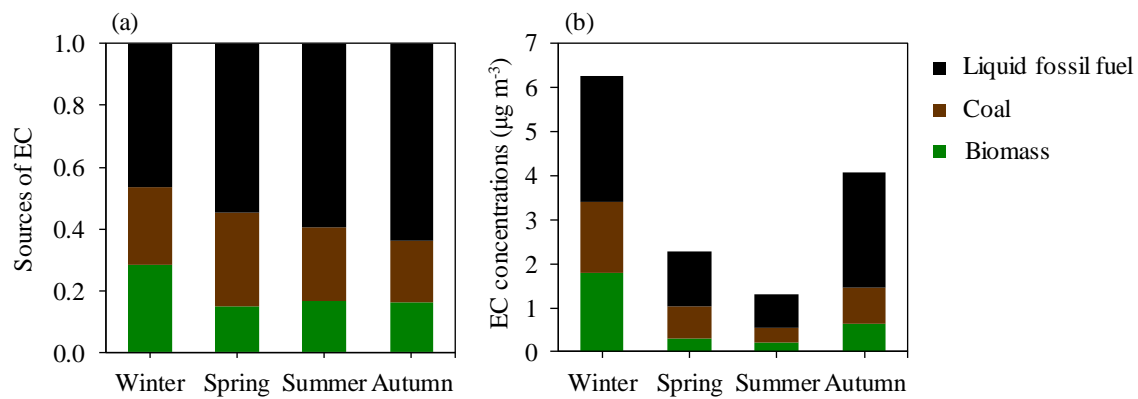
Figure 5. **(a)** Fractional contributions of 3 incomplete combustion sources to EC in different seasons. **(b)** Mass concentration of EC (μg m^{-3}) from each combustion source. The data are presented in Tables S7 and S8.
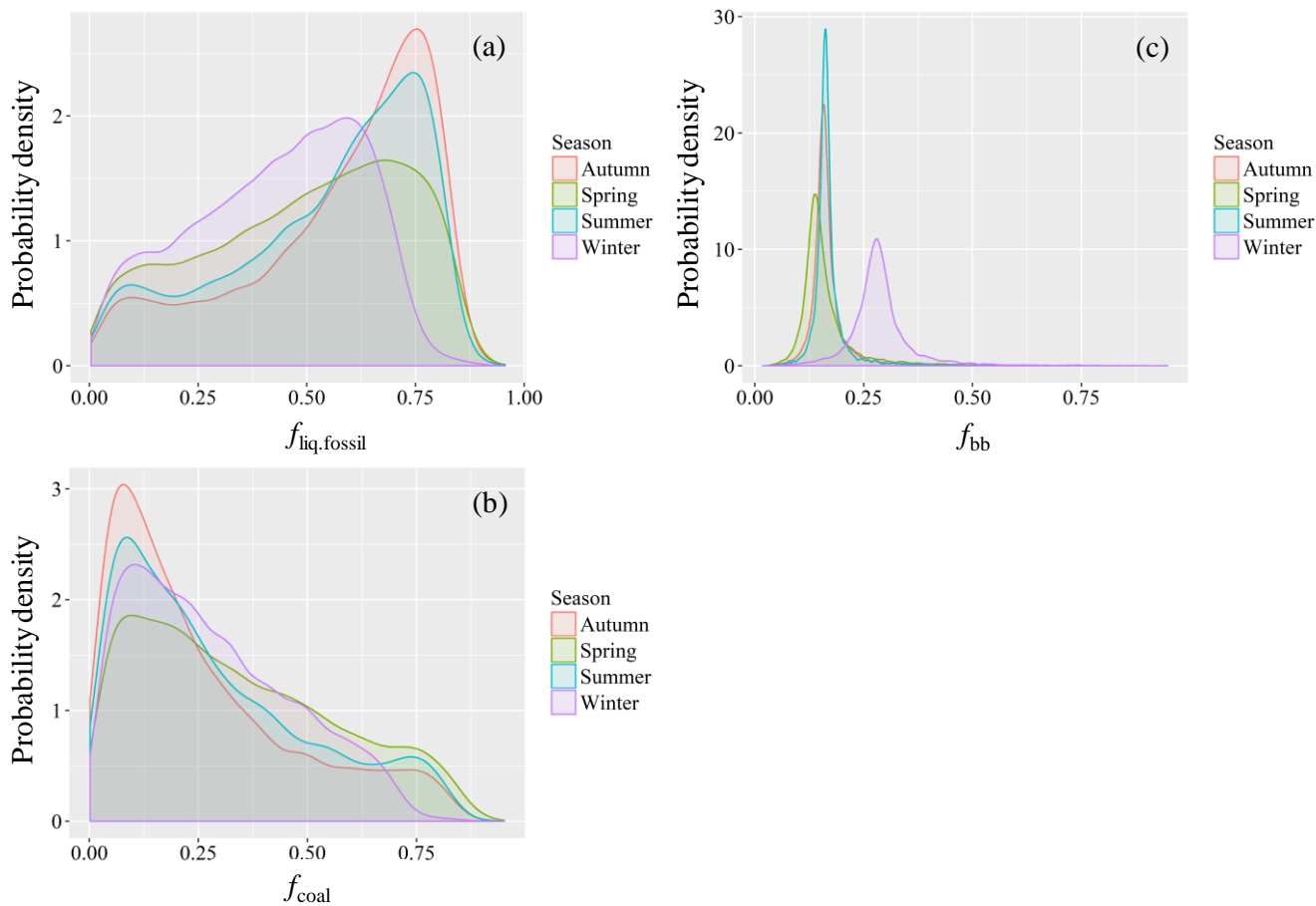
Figure 6. Probability density functions (PDFs) of the relative source contributions of **(a)** liquid fossil fuel combustion ($f_{liq.fossil}$), **(b)** coal combustion (f_{coal}) and **(c)** biomass burning (f_{bb}) to EC constrained by combining radiocarbon and $\delta^{13}C$ measurements, calculated using the Bayesian Markov chain Monte Carlo approach. For details, see Sect. 2.6.
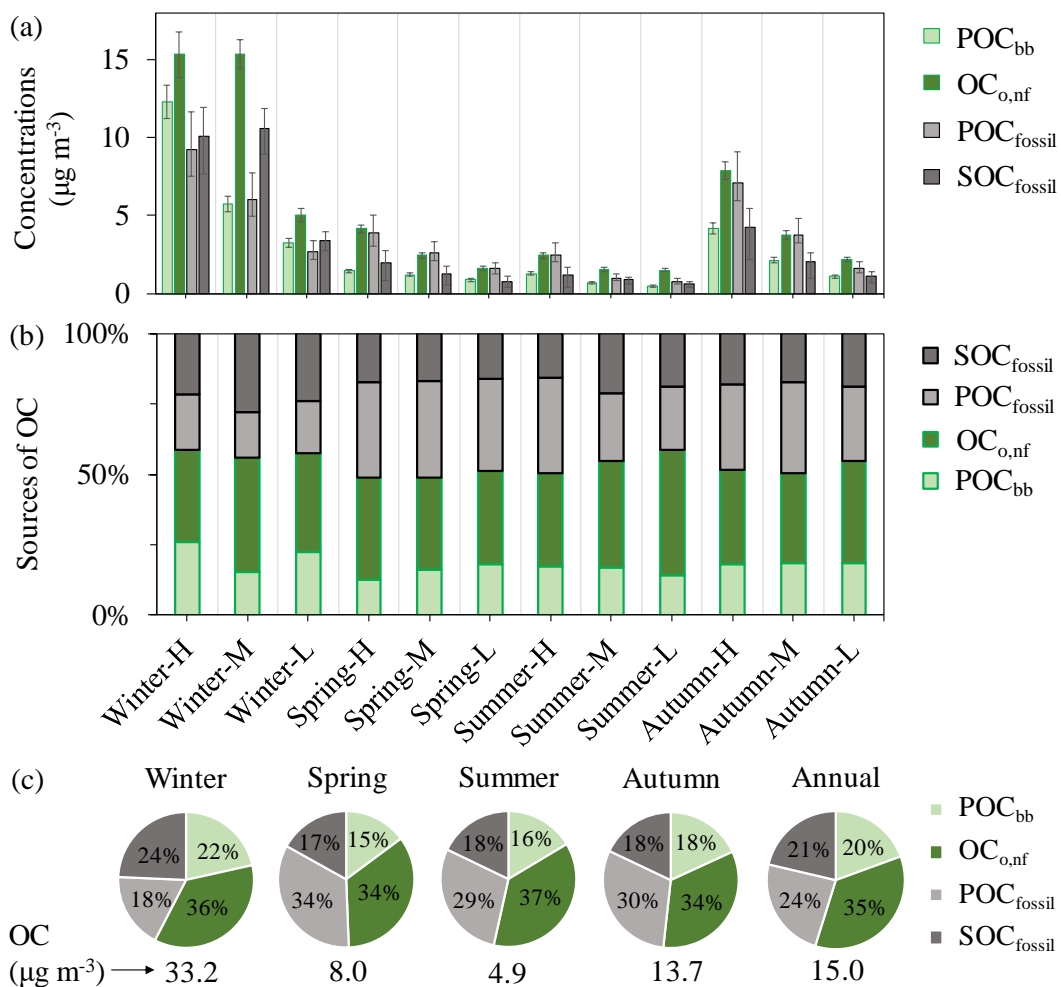
Figure 7. (a) The estimated mass concentrations of POC_{bb}, $OC_{o,nf}$, POC_{fossil}, SOC_{fossil} ($\mu g\ m^{-3}$) in total OC of $PM_{2.5}$ samples. The error bars indicate the interquartile range (25th–75th percentile) of the median values. (b) The percentage of POC_{bb}, $OC_{o,nf}$, POC_{fossil}, SOC_{fossil} in total OC. (c) Average source apportionment results of OC in each season and over the year. The numbers below the pie charts represent the seasonally/annually averaged OC concentrations.
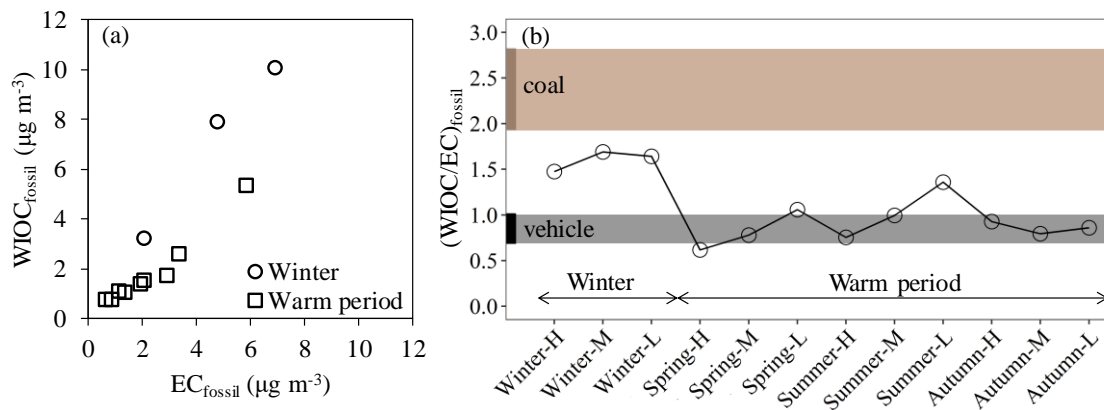
Figure 8. (a) A scatter plot of EC concentrations from fossil sources (EC$_{fossil}$) versus WIOC concentrations from fossil sources (WIOC$_{fossil}$) in winter (circle) and warm period (square). **(b)** The WIOC to EC ratio from fossil sources ((WIOC/EC)$_{fossil}$) over all the selected samples throughout the year. The dashed areas indicate typical primary OC/EC ratios for coal combustion (brown) and vehicle emissions (black).
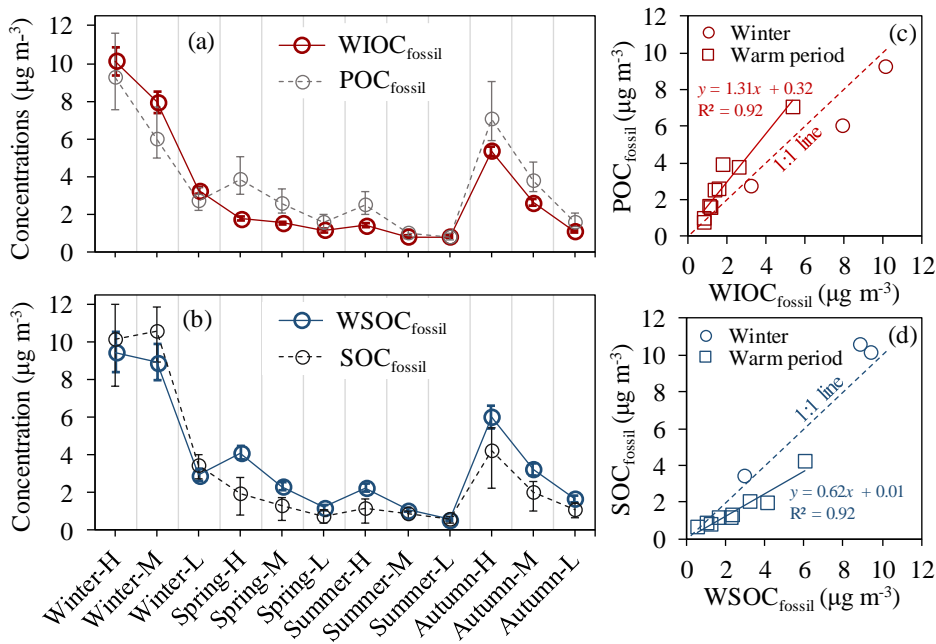
Figure 9. (**a**) Concentrations of WIOC and POC from fossil sources (WIOC$_{fossil}$ and POC$_{fossil}$, respectively)**.** Panel a has the same *x* axis with panel b. (**b**) Concentrations of WSOC and SOC from fossil sources (WSOC$_{fossil}$ and SOC$_{fossil}$, respectively)**. (c)** A scatter plot of WIOC$_{fossil}$ concentrations versus POC$_{fossil}$ concentrations. (**d**) A scatter plot of WSOC$_{fossil}$ concentrations versus SOC$_{fossil}$ concentrations. The interquartile range (25th-75th percentile) of the median POC$_{fossil}$ and SOC$_{fossil}$ is shown by grey vertical bars in panel a and black vertical bars in panel b.

Table 1. Relative contributions of non-fossil sources to EC, OC, WIOC and WSOC (f_{bb}(EC), f_{nf}(OC), f_{nf}(WIOC), f_{nf}(WSOC)), and relative fossil sources contribution to EC, OC, WIOC and WSOC (f_{fossil}(EC), f_{fossil}(OC), f_{fossil}(WIOC), f_{fossil}(WSOC)) for each sample.

Sample name	f_{bb}(EC)	f_{fossil}(EC)	f_{nf}(OC)	f_{fossil}(OC)	f_{nf}(WIOC)	f_{fossil}(WIOC)	f_{nf}(WSOC)	f_{fossil}(WSOC)
Winter-H	0.310 ± 0.008	0.690 ± 0.008	0.587 ± 0.014	0.413 ± 0.014	0.516 ± 0.012	0.484 ± 0.012	0.639 ± 0.014	0.361 ± 0.014
Winter-M	0.235 ± 0.006	0.765 ± 0.006	0.559 ± 0.012	0.441 ± 0.012	0.509 ± 0.012	0.491 ± 0.012	0.590 ± 0.012	0.410 ± 0.012
Winter-L	0.291 ± 0.007	0.709 ± 0.007	0.574 ± 0.012	0.426 ± 0.012	0.504 ± 0.011	0.496 ± 0.011	0.627 ± 0.013	0.373 ± 0.013
Spring-H	0.112 ± 0.004	0.888 ± 0.004	0.490 ± 0.011	0.510 ± 0.011	0.468 ± 0.011	0.532 ± 0.011	0.495 ± 0.010	0.505 ± 0.010
Spring-M	0.132 ± 0.006	0.868 ± 0.006	0.487 ± 0.011	0.513 ± 0.011	0.410 ± 0.010	0.590 ± 0.010	0.525 ± 0.011	0.475 ± 0.011
Spring-L	0.167 ± 0.005	0.833 ± 0.005	0.511 ± 0.011	0.489 ± 0.011	0.406 ± 0.010	0.594 ± 0.010	0.578 ± 0.014	0.422 ± 0.014
Summer-H	0.144 ± 0.005	0.856 ± 0.005	0.504 ± 0.011	0.496 ± 0.011	0.399 ± 0.009	0.601 ± 0.009	0.550 ± 0.012	0.450 ± 0.012
Summer-M	0.173 ± 0.005	0.827 ± 0.005	0.544 ± 0.012	0.456 ± 0.012	0.454 ± 0.010	0.546 ± 0.010	0.591 ± 0.013	0.409 ± 0.013
Summer-L	0.165 ± 0.006	0.835 ± 0.006	0.585 ± 0.012	0.415 ± 0.012	0.359 ± 0.009	0.641 ± 0.009	0.720 ± 0.019	0.280 ± 0.019
Autumn-H	0.153 ± 0.005	0.847 ± 0.005	0.516 ± 0.011	0.484 ± 0.011	0.470 ± 0.011	0.530 ± 0.011	0.545 ± 0.011	0.455 ± 0.011
Autumn-M	0.140 ± 0.004	0.860 ± 0.004	0.502 ± 0.011	0.498 ± 0.011	0.448 ± 0.010	0.552 ± 0.010	0.534 ± 0.011	0.466 ± 0.011
Autumn-L	0.177 ± 0.005	0.823 ± 0.005	0.544 ± 0.012	0.456 ± 0.012	0.472 ± 0.011	0.528 ± 0.011	0.578 ± 0.012	0.422 ± 0.012